Approaching complete low-spin spectroscopy of ^{210}Bi with a cold-neutron capture reaction

N. Cieplicka-Oryńczak,[1,2] B. Fornal,[2] S. Leoni,[1,3] D. Bazzacco,[4] A. Blanc,[5] G. Bocchi,[3] S. Bottoni,[3] G. de France,[6] M. Jentschel,[5] U. Köster,[5] P. Mutti,[5] G. Simpson,[7] T. Soldner,[5] B. Szpak,[2] C. Ur,[8] and W. Urban[9]

[1]*INFN Sezione di Milano, Via Celoria 16, 20133 Milano, Italy*

[2]*Institute of Nuclear Physics, Polish Academy of Sciences, PL-31342 Kraków, Poland*

[3]*Università degli Studi di Milano, Via Celoria 16, 20133 Milano, Italy*

[4]*Dipartimento di Fisica e Astronomia dell'Università and INFN Sezione di Padova, I-35131 Padova, Italy*

[5]*Institute Laue-Langevin, 6 rue Jules Horowitz, 38042 Grenoble Cedex 9, France*

[6]*GANIL, Boulevard Becquerel, BP 55027, 14076 CAEN Cedex 05, France*

[7]*LPSC, Université Joseph Fourier Grenoble 1, CNRS/IN2P3, Institut National Polytechnique de Grenoble, F-38026 Grenoble Cedex, France*

[8]*INFN Sezione di Padova, Via F. Marzolo 8, I-35131 Padova, Italy*

[9]*Faculty of Physics, University of Warsaw, ulica Hoża 69, 02681 Warszawa, Poland*

(Received 19 October 2015; published 2 May 2016)

The low-spin structure of the ^{210}Bi nucleus was investigated in the neutron capture experiment ^{209}Bi$(n,\gamma)^{210}$Bi performed at ILL Grenoble at the PF1B cold-neutron facility. By using the EXILL multidetector array, consisting of 46 high-purity germanium crystals, and $\gamma\gamma$-coincidence technique, 64 primary γ rays were observed (40 new) and a total number of 70 discrete states (33 new) were located below the neutron binding energy in ^{210}Bi. The analysis of the angular correlations of γ rays provided information about transitions multipolarities, which made it possible to confirm most of the previously known spin-parity assignments and helped establish new ones. The obtained experimental results were compared to shell-model calculations involving one-valence-proton, one-valence-neutron excitations outside the ^{208}Pb core. It has been found that while up to the energy of ∼2 MeV each state observed in ^{210}Bi has its calculated counterpart; at higher excitation energies some levels cannot be described by the valence particle couplings. These states may arise from couplings of valence particles to the 3^- octupole phonon of the doubly magic ^{208}Pb core and may serve as a testing ground for models which describe single particle-phonon excitations.

DOI: 10.1103/PhysRevC.93.054302

I. INTRODUCTION

The ^{210}Bi nucleus belongs to the region surrounding one of the best-known doubly magic nuclei: ^{208}Pb. ^{210}Bi is a one-valence-proton, one-valence-neutron nucleus; thus, it may serve as a favorable testing ground for theoretical calculations involving proton-neutron excitations and couplings of particles with excitations of the core. The low-energy structure of ^{210}Bi, up to ∼2 MeV, should arise exclusively from couplings of a proton on the $1h_{9/2}$, $2f_{7/2}$, $1i_{13/2}$, $2f_{5/2}$, $3p_{3/2}$, $3p_{1/2}$ orbitals and a neutron on the $2g_{9/2}$, $1i_{11/2}$, $1j_{15/2}$, $3d_{5/2}$, $4s_{1/2}$, $2g_{7/2}$, $3d_{3/2}$ orbitals, while at higher energies states that originate from the couplings between valence particles and the 3^- octupole vibration of ^{208}Pb (at 2615 keV) should appear. Over the years, several experimental investigations have been performed providing partial information on different regions of spin and excitation energy. The ground state of ^{210}Bi was proven to have spin parity $J^\pi = 1^-$ and to belong to the fully identified multiplet $\pi h_{9/2}\nu g_{9/2}$ [1], while the member of this multiplet with maximum spin, $J^\pi = 9^-$, lies at 271 keV and is the second excited state in this nuclide. Owing to the large spin difference, the 9^- excitation is a long-lived, α-decaying isomer with $T_{1/2} = 3.04 \times 10^6$ yr. The presence of two other isomeric excitations belonging to the same multiplet, a $J^\pi = 7^-$ state at 433 keV with $T_{1/2} = 57.5$ ns and a $J^\pi = 5^-$ excitation at 439 keV with $T_{1/2} = 37.7$ ns, together with the remaining members with $J^\pi = 2^-,3^-,4^-$, and 6^-, was reported in Ref. [2]. Other proton-neutron multiplets have been identified in this nucleus as well. For example, a complete set of states arising from the $\pi h_{9/2}\nu i_{11/2}$ and $\pi f_{7/2}\nu g_{9/2}$ couplings were found in different reactions [3]; the excited states in ^{210}Bi were traced up to levels at ∼4.2 MeV and spin range from $1\hbar$ to $14\hbar$. In addition, the high-spin yrast states up to 6 MeV [and the highest spin value of (19^-) assigned for the 4965-keV level] were studied with heavy-ion reactions by Cieplicka *et al.* [4].

Measurements with thermal neutron capture reactions [5–7] reported a series of findings below the neutron binding energy of ^{210}Bi (i.e., 4604.63 keV [8]). In the work of Tsai *et al.* [6], 16 states up to 2 MeV were established based on the observation of high-energy primary γ rays. The presence of two components of the capture state (4^- and 5^-) was deduced as well. A more detailed investigation was performed by Sheline *et al.* [5]: 57 states up to 3.2 MeV were found by analyzing the γ-ray spectrum collected with one Ge detector. Next, in the most recent paper of Borella *et al.* [7] a few tens of new levels were located [3], although not for all of them could spin and parity be assigned.

Taking it all together, in the neutron capture studies performed so far, levels up to the 3244-keV excitation energy were located and 27 primary γ rays deexciting the capture state were observed. One should be aware that these investigations were performed without employing γ-ray coincidence techniques, thus limiting the observation and placement of weak transitions. It was clear that by using a highly efficient multidetector Ge array, one could perform a much more detailed spectroscopic investigation of ^{210}Bi at low spins.

In this work, we have performed a study of the decay of ^{210}Bi populated in a cold-neutron capture reaction at Institut Laue-Langevin (ILL) at Grenoble, making use of the highly efficient EXILL (EXOGAM at ILL) multidetector array [9]. Sixty-four primary γ rays were observed (40 new) and a total number of 70 discrete states (33 new) were located below the neutron binding energy in ^{210}Bi. Spin-parity assignments for most of the newly identified states were established based on their decay pattern and angular correlations. It is anticipated that the present experimental work, together with previous investigations, makes it possible to approach complete spectroscopy in ^{210}Bi at low spins ($J < 8$). This provides a unique opportunity for a one-to-one comparison with theoretical calculations for the entire energy range, from the ground state to the neutron binding energy.

Section II, where the experimental procedure and results are presented, includes two parts: the construction of the level scheme (Sec. II A) and the angular correlations and multipolarity determinations (Sec. II B). The third section provides the comparisons of the experimental results with predictions based on shell-model calculations involving the presently available two-body shell-model interactions; the possible spin-parity assignments are discussed as well. Section IV contains conclusions and summary.

II. EXPERIMENTAL PROCEDURE AND RESULTS

A. Construction of the level scheme

The experiment was performed at the PF1B cold-neutron facility [10] at the Institut Laue-Langevin in Grenoble. The neutron beam from the ILL reactor, after traveling through the collimation line, had a diameter of 12 mm and the capture flux was about $10^8/(\mathrm{s} \times \mathrm{cm}^2)$ at the target position. The target was made of ^{209}Bi pieces (total weight of 3 g), cylindrically shaped in a Teflon bag, placed in the center of the EXILL array. This array consisted of 16 high-purity germanium (HPGe) detectors: 8 EXOGAM (GAMma-ray from EXOtic nuclei spectrometer) clover detectors [11], 6 GASP (GAmma-ray SPectrometer) detectors [12] with their Bismuth Germanium Oxide anti-Compton suppressors, as well as two clovers from the ILL LOHENGRIN Instrument. This is the first time such a highly efficient HPGe setup (with efficiency of ≈6%) was used at a neutron beam facility. The detailed description of

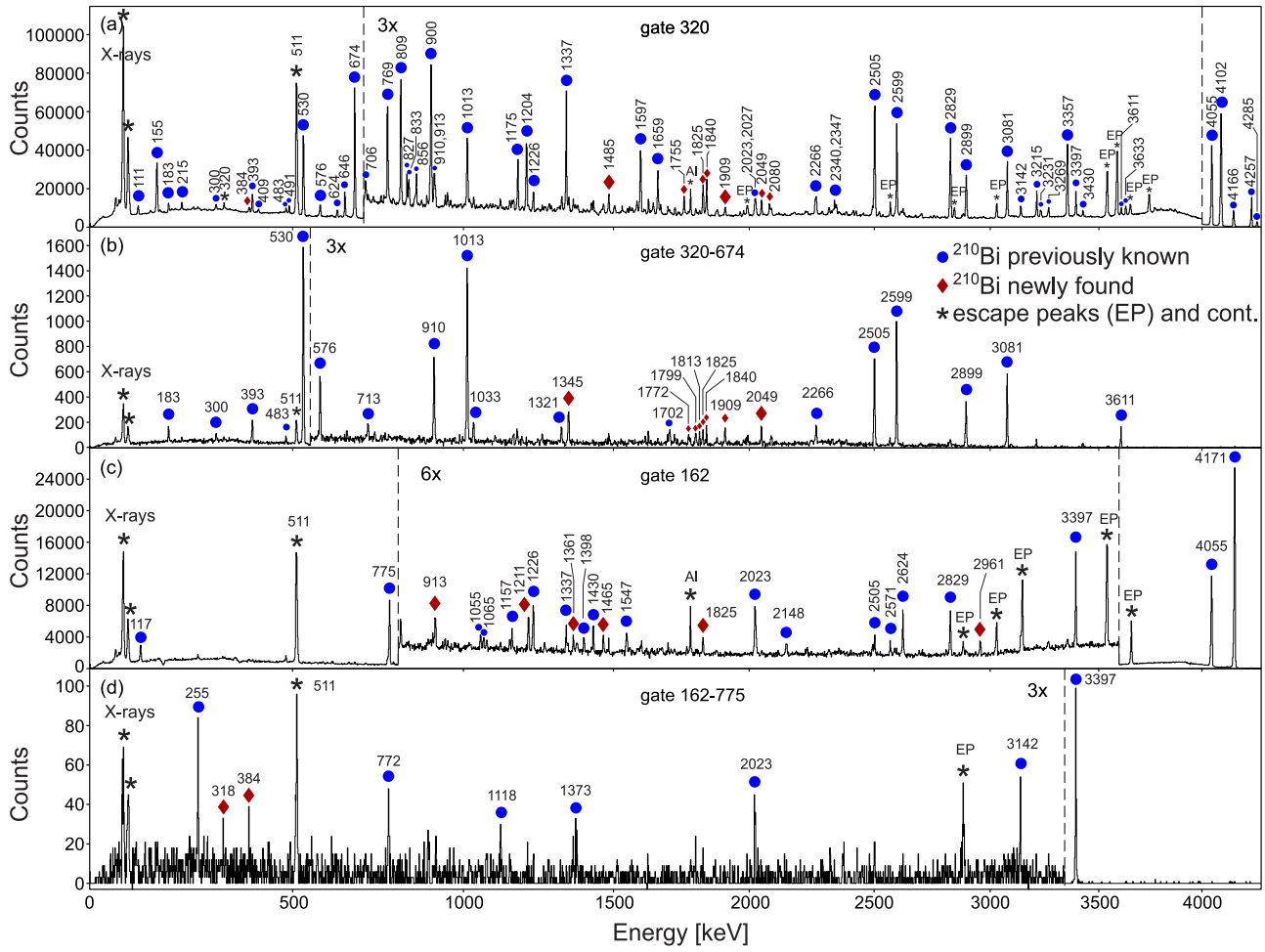

FIG. 1. Representative coincidence spectra for ^{210}Bi. (a) Spectrum single-gated on the 320-keV transition; (b) spectrum double-gated on the pair of transitions at 320 and 674 keV; (c) spectrum single-gated on the 162-keV transition; (d) spectrum double-gated on the 162- and 775-keV transitions.

the experimental setup and characteristics may be found in Ref. [9].

To collect and process the signals from the detectors, digital electronics was used and the data were stored triggerless. The events contained information about γ-ray energy, the time of the registration (with a time stamp every 10 ns) and the identification number of the specific detector that fired [13].

The neutron capture reaction leads to ^{210}Bi, which then decays through emission of γ-ray cascades. As the measured γ spectrum was very complex owing to a large number of decay paths, the γ-coincidence technique was applied. The collected data were sorted offline into a $\gamma\gamma$-coincidence matrix and a $\gamma\gamma\gamma$-coincidence cube with a coincidence time window of 200 ns. The energy calibration was done based on the contaminant strong peaks from ^{28}Al and ^{36}Cl isotopes. The procedures of time and energy calibration are described in detail in Ref. [14]. The gating on the already known, low-spin transitions in ^{210}Bi made it possible to produce coincidence spectra, the analysis of which resulted in building the level scheme of this nucleus below the neutron capture state. Although only ^{210}Bi was produced in this reaction (apart from small number of contaminants), the collected data contain many γ transitions, owing to the large number of primary γ rays feeding numerous states. Thus, to build a complex level scheme, the analysis required identification of various paths of the decay. This was done by inspection of a large number of coincidence spectra; examples are presented in Figs. 1 and 2.

The ^{210}Bi decay scheme established in the present studies is given in Fig. 3 (showing only the primary γ rays), 4, 5, and 6. Because this is the first time a multidetector HPGe array was used for the coincidence measurements of γ rays from cold-neutron capture on ^{210}Bi, the whole previously known scheme has been revised. The γ energies observed thus far are marked in black (even if their placement has been changed), while the newly found transitions are shown in red. The building of the level structure started from producing spectra of γ rays coincident with the strong γ transitions previously observed in the lowest part of the scheme, i.e., the 320-keV ($2^- \rightarrow 1^-$) γ ray feeding the ground state [Fig. 1(a)] or the 162-keV ($7^- \rightarrow 9^-$) transition populating the long-lived isomeric state [Fig. 1(c)]. These histograms were generated by using the $\gamma\gamma$ matrix, and the resulting spectra were very complex; they displayed a large amount of lines belonging to ^{210}Bi. Only at higher energies was the density of lines relatively low. For example, the two peaks at 4285 and 4171 keV, associated with transitions from the 4605-keV state to the first 2^- and 7^- levels at 320 and 433 keV, respectively, could be easily seen in the 320- and 162-keV-gated spectra [Figs. 1(a) and 1(c)]. Moreover, setting gates on the other such high-energy γ rays makes it possible to clean the spectra and easily identify the main paths of the decay. For example, the spectrum gated on the 2599-keV primary transition [Fig. 2(a)] shows three strongest γ rays—1013, 674, and 320 keV—which belong to a cascade originating from the 2007-keV state through 993- and 320-keV levels to the ground state. A few intense peaks are also visible in the spectrum gated on the 3397-keV line [Fig. 2(b)], which is a primary γ ray leading to the 1209-keV level. The two strongest paths defined by the 769- and 775-keV lines lead further through the 91-28-320-keV cascade and 162-keV

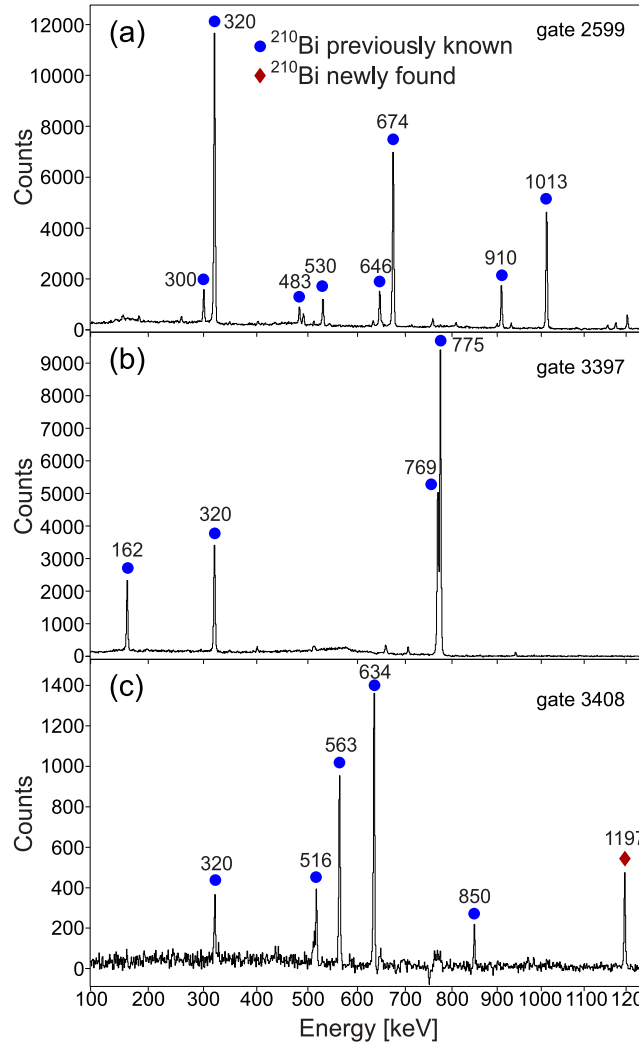

FIG. 2. Representative coincidence single-gated spectra for ^{210}Bi. The gates were set on the high-energy primary γ rays specified in the labels of each panel, which significantly cleaned the spectra.

transition to the ground and long-lived isomeric states, respectively. In the spectrum gated on the 3408-keV γ ray (this primary transition should populate a state at 1197 keV of which no γ decay was reported previously), shown in Fig. 2(c), one can notice two strongest peaks: 563 and 634 keV. From the energy differences between the levels one can deduce that the 634-keV γ ray feeds the 563-keV level, which deexcites then by the 563- and 517-keV lines. Similarly, the 850- and 1197-keV transitions may lead to the 348-keV level and the ground state, respectively. The spectra gated on the other transitions are in line with this scenario. However, to confirm the previous level scheme and to perform a search for new transitions, the $\gamma\gamma\gamma$-coincidence cube had to be used.

The analysis involved inspection of many spectra gated on different combinations of γ rays. In particular, a search for coincident transitions energies that would sum up to 4605 keV (when feeding the 320-keV state) or 4334 keV (when feeding the 271-keV state) was performed (some transitions could, of course, be coincident with both 320- and 162-keV lines).

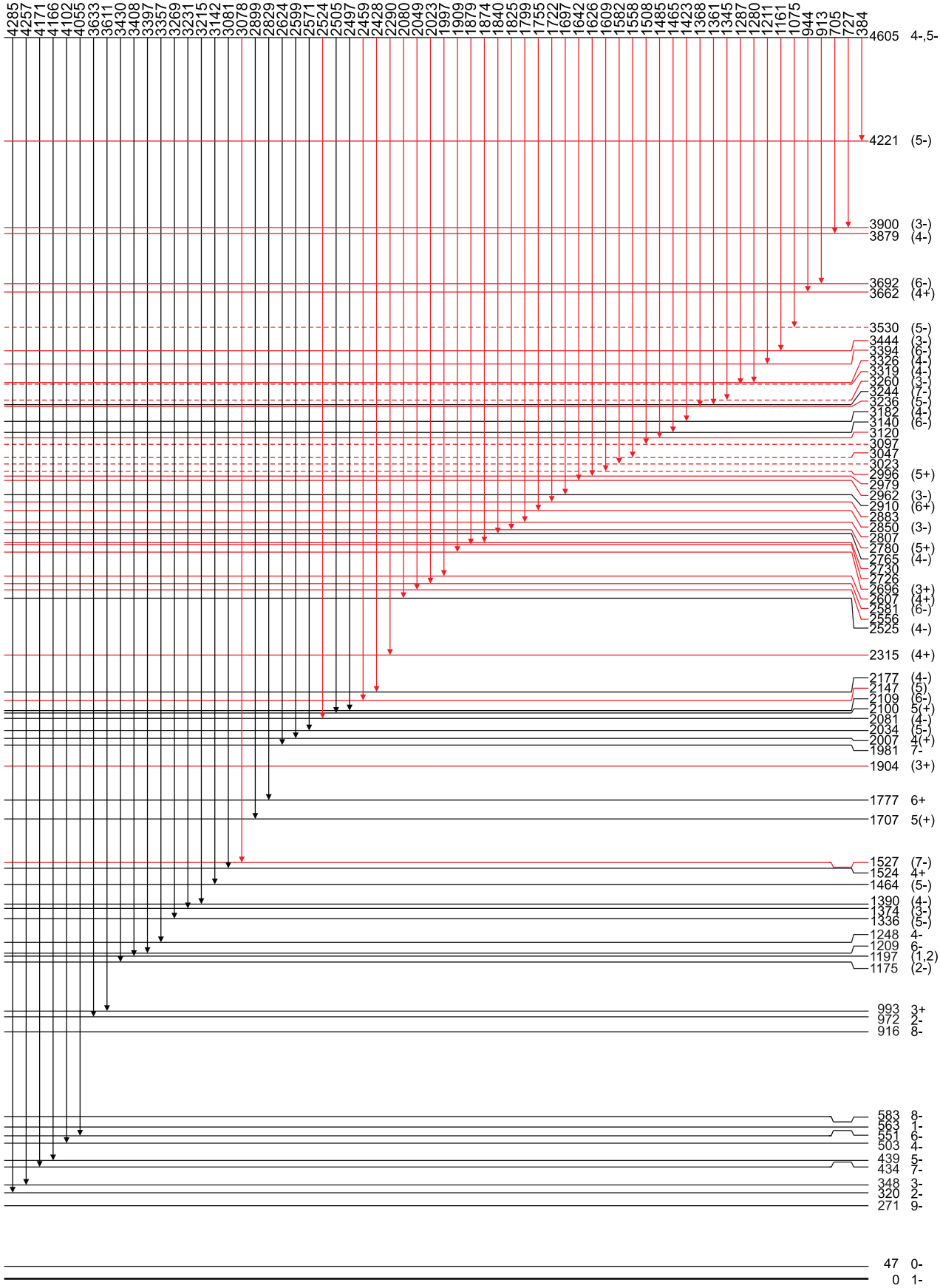

FIG. 3. Primary γ rays from the capture state at 4.6 MeV (4^-,5^-) in ^{210}Bi. The dashed lines indicate tentatively identified levels.

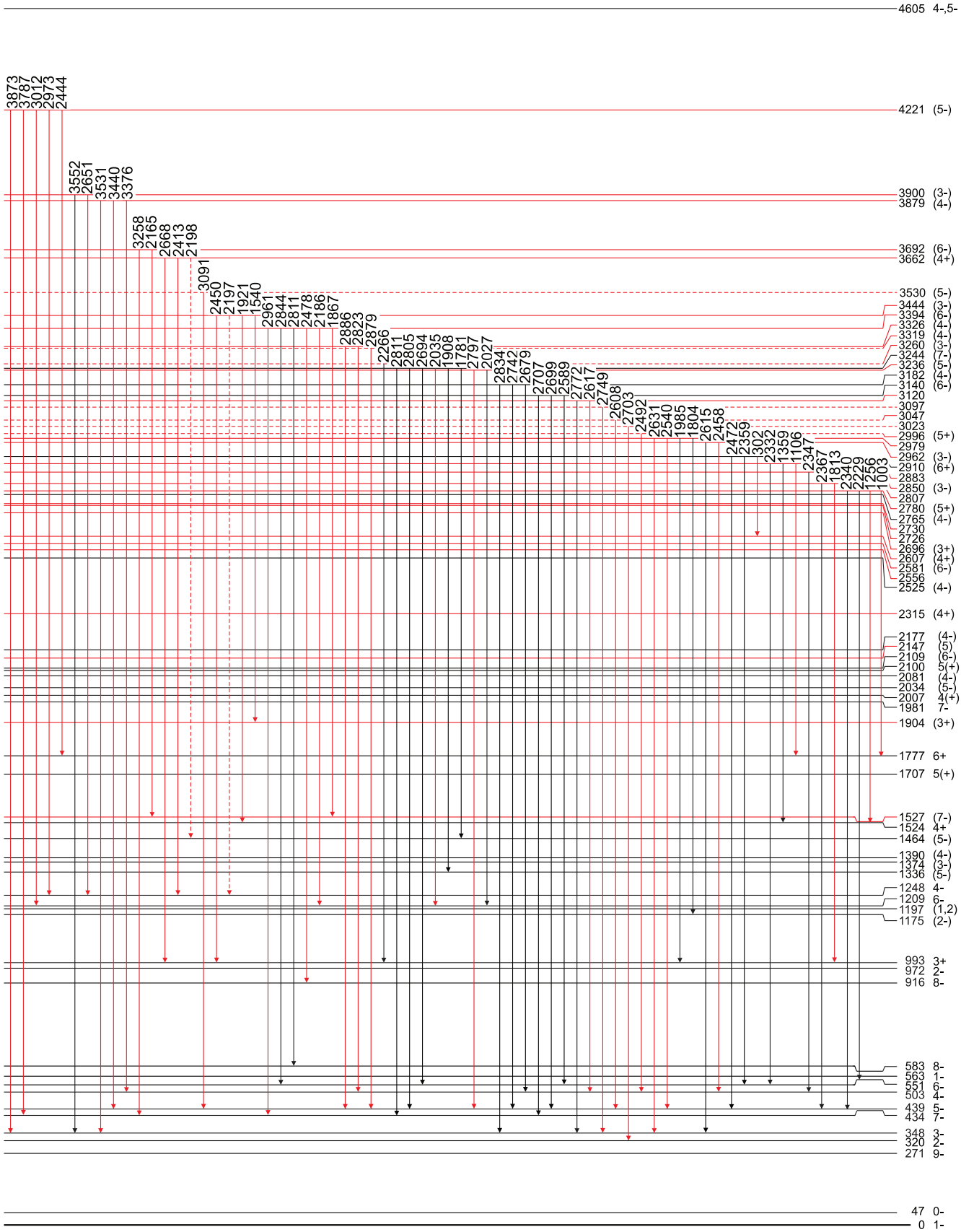

FIG. 4. Level scheme of ^{210}Bi displaying the transitions which follow primary γ rays from the capture state, shown in Fig. 3, established in the present work. The newly found levels and γ rays are marked in red. The dashed lines indicate tentatively identified levels.

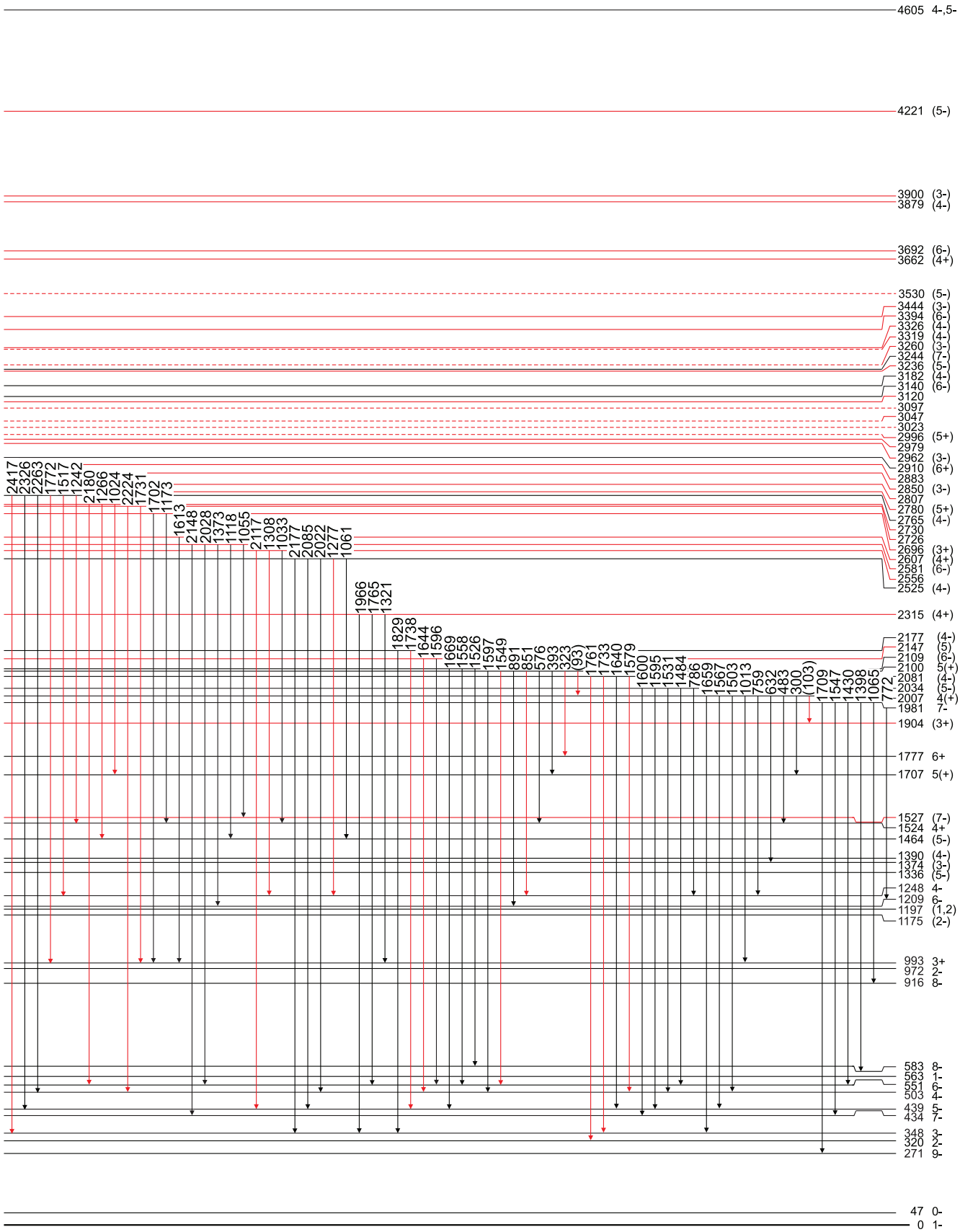

FIG. 5. Level scheme of ^{210}Bi displaying the transitions which follow primary γ rays from the capture state, shown in Fig. 3, established in the present work. The newly found levels and γ rays are marked in red. The dashed lines indicate tentatively identified levels.

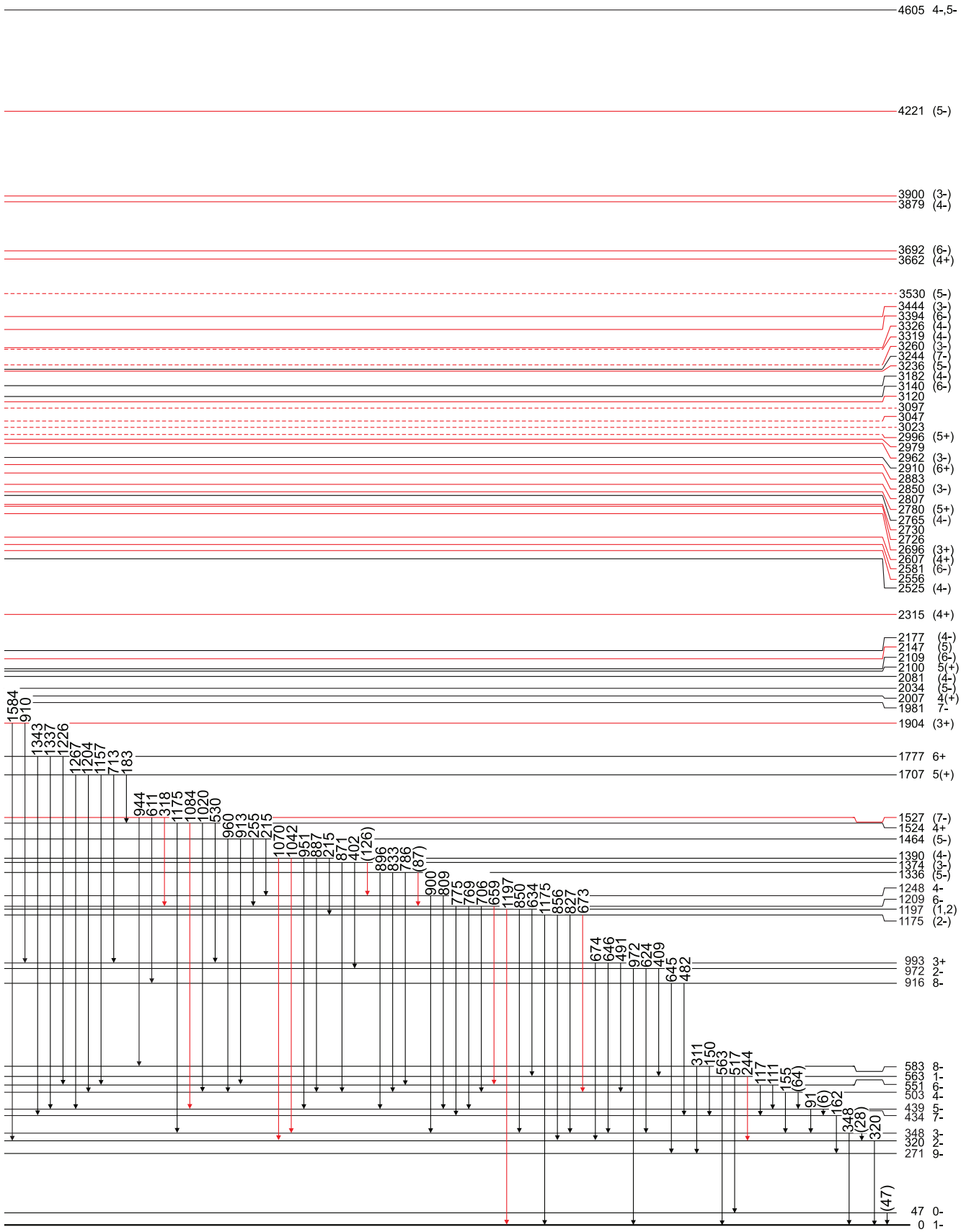

FIG. 6. Level scheme of ^{210}Bi displaying the transitions which follow primary γ rays from the capture state, shown in Fig. 3, established in the present work. The newly found levels and γ rays are marked in red. The dashed lines indicate tentatively identified levels.

TABLE I. Information on levels and transitions in ^{210}Bi from the present experiment. In the first four columns the energies and spin-parities of the initial and final states are given. Newly found levels are labeled by "*new*". Column 5 provides the energies of γ rays while γ-ray branching ratios BR_γ are presented in the last column. The sixth column provides the theoretical values of conversion coefficients α, used in some cases to calculate the branching ratios for the low-energy γ rays, together with the assumed multipolarities for those transitions (the lowest possible order of multipole was assumed in each case). Column 7 gives the multipolarities of transitions analyzed in the present experiment (see Sec. II B).

E_i (keV)	J_i^π	E_f (keV)	J_f^π	E_γ (keV)	α ($M\lambda, E\lambda$)	Multipolarity	BR_γ
47	0^-	0	1^-	46.8(2)[d]	17.56 ($M1$)		0.054[e]
271[a]	9^-						
320	2^-	0	1^-	319.9(1)	0.39 ($M1$)	$M1(+E2)$	0.720
348	3^-	320	2^-	28.2(7)[d]	78.3 ($M1$)		0.012(8)[e]
		0	1^-	348.1(7)	0.08 ($E2$)	$E2$	0.012(9)
434	7^-	271	9^-	162.5(1)	0.96 ($E2$)		0.509
439	5^-	434	7^-	5.7(12)[d]	2×10^6 ($E2$)		0.0
		348	3^-	91.4(9)	9.61 ($E2$)		0.081(51)
503	4^-	439	5^-	63.7(17)[d]	7.11 ($M1$)		0.03(3)[e]
		348	3^-	155.1(2)	2.92 ($M1$)		0.198(145)
551	6^-	439	5^-	111.1(1)	7.56 ($M1$)		0.052(37)
		434	7^-	116.9(1)	6.51 ($M1$)		0.074(53)
563	1^-	320	2^-	243.9(2)	0.82 ($M1$)		0.053(37)
		47	0^-	516.8(1)	0.11 ($M1$)		0.194(136)
		0	1^-	563.4(1)	0.09 ($M1$)	$M1(+E2)$	0.634(444)
583	8^-	434	7^-	149.7(2)	3.21 ($M1$)		0.102(71)
		271	9^-	311.4(1)	0.42 ($M1$)	$M1(+E2)$	0.403(274)
916	8^-	434	7^-	482.3(1)	0.13 ($M1$)		0.293(207)
		271	9^-	644.6(1)	0.06 ($M1$)	($M1$)	0.631(451)
972	2^-	563	1^-	409.0(1)	0.20 ($M1$)	$M1$	0.356(216)
		348	3^-	624.1(1)	0.07 ($M1$)		0.095(59)
		0	1^-	972.0(1)			0.462(118)
993	3^+	503	4^-	491.0(1)			0.038(22)
		348	3^-	646.0(1)			0.153(89)
		320	2^-	674.1(1)		$E1(+M2)$	0.803(97)
1175	(2^-)	503	4^-	672.7(2)			0.203(18)
		348	3^-	827.4(1)			0.374(31)
		320	2^-	855.6(1)			0.380(31)
		0	1^-	1174.5(5)			0.016(4)
1197	(1,2)	563	1^-	634.2(1)		$\Delta J = 1$	0.645(439)
		348	3^-	849.5(2)			0.095(36)
		0	1^-	1197.2(1)			0.260(99)
1209	6^-	551	6^-	658.5(2)	0.06 ($M1$)		0.016(2)
		503	4^-	705.6(2)			0.016(2)
		439	5^-	769.4(1)		$\Delta J = 1$	0.358(47)
		434	7^-	775.1(2)		$\Delta J = 1$	0.574(70)
1248	4^-	439	5^-	808.9(1)		$M1(+E2)$	0.528(41)
		348	3^-	900.2(1)			0.443(35)
1336	(5^-)	1209	6^-	127.2(8)[d]	5.15 ($M1$)		0.036(29)[e]
		551	6^-	786.1(2)			0.206(43)
		503	4^-	832.7(1)			0.334(68)
		439	5^-	896.4(1)			0.239(58)
1374	(3^-)	1248	(4^-)	126.1(9)[d]	5.27 ($M1$)		0.028(25)[e]
		972	2^-	402.3(1)	0.21 ($M1$)		0.578(403)
		503	4^-	871.3(1)			0.124(52)
1390	(4^-)	1175	(2^-)	215.1(1)	0.35 ($E2$)		0.351(217)
		503	4^-	887.2(1)			0.173(47)
		439	5^-	950.8(1)		$M1(+E2)$	0.256(70)
		348	3^-	1042.1(1)			0.064(18)
		320	2^-	1070.4(3)			0.022(6)
1464	(5^-)	1248	(4^-)	215.4(2)	1.17 ($M1$)		0.122(75)
		1209	6^-	254.8(1)	0.73 ($M1$)		0.207(126)

TABLE I. (*Continued.*)

E_i (keV)	J_i^π	E_f (keV)	J_f^π	E_γ (keV)	$\alpha\,(M\lambda, E\lambda)$	Multipolarity	BR_γ
		551	6^-	913.1(1)			0.283(73)
		503	4^-	960.4(2)			0.087(23)
1524	4^+	993	3^+	529.9(1)	0.10 ($M1$)	$M1(+E2)$	0.668(468)
		503	4^-	1020.3(1)			0.026(11)
		439	5^-	1084.3(3)			0.013(6)
		348	3^-	1175.3(1)		($E1$)	0.226(95)
1527 *new*	(7^-)	1209	6^-	318.4(4)	0.40 ($M1$)		0.091(61)
		916	8^-	611.0(1)	0.07 ($M1$)	($M1$)	0.536(355)
		583	8^-	944.2(1)			0.293(101)
1707	$5(^+)$	1524	4^+	183.4(1)	1.83 ($M1$)		0.162(100)
		993	3^+	712.8(2)			0.031(8)
		551	6^-	1156.5(1)			0.108(29)
		503	4^-	1203.7(1)		$E1(+M2)$	0.383(102)
		439	5^-	1267.3(2)			0.019(5)
1777	6^+	551	6^-	1226.4(1)			0.234(25)
		439	5^-	1337.2(1)		$E1(+M2)$	0.738(102)
		434	7^-	1342.6(2)			0.028(13)
1904 *new*	(3+)	993	3^+	909.8(1)			0.755(68)
		320	2^-	1583.7(1)			0.245(23)
1981	7^-	1209	6^-	772.3(1)			0.045(7)
		916	8^-	1064.7(1)		$M1(+E2)$	0.096(8)
		583	8^-	1398.0(1)		$M1(+E2)$	0.192(15)
		551	6^-	1430.3(1)		$M1(+E2)$	0.187(14)
		434	7^-	1546.8(1)			0.068(5)
		271	9^-	1709.0(1)		$E2$	0.411(31)
2007	$4(^+)$	1904	(3+)	103.1(4)[d]	9.36 ($M1$)		0.014(11)[e]
		1707	$5(^+)$	300.0(1)	0.46 ($M1$)		0.070(40)
		1524	4^+	483.1(1)	0.13 ($M1$)		0.033(19)
		1374	(3^-)	632.4(2)			0.012(7)
		1248	(4^-)	758.7(1)			0.021(3)
		993	3^+	1012.6(1)		$(M1 + E2)$	0.339(50)
		503	4^-	1503.4(1)			0.040(6)
		439	5^-	1567.2(1)			0.029(4)
		348	3^-	1658.8(1)		$E1(+M2)$	0.273(41)
2034	(5^-)	1248	(4^-)	785.9(4)			0.040(3)
		551	6^-	1483.9(1)		$M1(+E2)$	0.435(37)
		503	4^-	1531.1(1)			0.198(19)
		439	5^-	1594.6(2)			0.175(24)
		434	7^-	1600.4(2)			0.153(22)
2081	(4^-)	503	4^-	1578.5(8)			0.141(55)
		439	5^-	1640.3(5)			0.220(43)
		348	3^-	1732.5(2)			0.341(47)
		320	2^-	1761.0(3)			0.299(39)
2100	$5(^+)$	2007	$4(^+)$	93.0(4)[d]	12.44($M1$)		0.011(8)[e]
		1777	6^+	322.5(9)	0.38 ($M1$)		0.028(22)
		1707	$5(^+)$	393.0(1)	0.22 ($M1$)	$\Delta J = 0$	0.191(112)
		1524	4^+	576.2(1)	0.08 ($M1$)		0.119(71)
		1248	(4^-)	851.3(1)			0.031(6)
		1209	6^-	890.8(1)			0.034(7)
		551	6^-	1549.4(1)			0.040(8)
		503	4^-	1596.5(1)		$\Delta J = 1$	0.351(75)
2109	(6^-)	583	8^-	1526.0(2)			0.191(18)
		551	6^-	1558.1(1)			0.179(19)
		439	5^-	1669.1(1)			0.630(59)
2147 *new*	(5)	551	6^-	1596.1(2)			0.432(56)
		503	4^-	1643.8(2)			0.568(67)
2177	(4^-)	439	5^-	1737.7(2)			0.527(53)

TABLE I. (*Continued.*)

E_i (keV)	J_i^π	E_f (keV)	J_f^π	E_γ (keV)	$\alpha\,(M\lambda, E\lambda)$	Multipolarity	BR_γ
		348	3^-	1829.1(1)			0.473(47)
2315 *new*	(4^+)	993	3^+	1321.1(2)			0.356(38)
		551	6^-	1765.0(2)			0.291(33)
		348	3^-	1966.4(3)			0.353(38)
2525	(4^-)	1464	(5^-)	1061.3(1)			0.172(16)
		1248	(4^-)	1276.5(2)			0.143(14)
		503	4^-	2021.7(1)			0.351(32)
		439	5^-	2085.2(2)			0.170(16)
		348	3^-	2176.5(2)			0.164(16)
2556 *new*	[b]	1524	4^+	1032.8(1)			0.549(45)
		1248	(4^-)	1308.1(2)			0.210(20)
		439	5^-	2117.0(2)			0.241(24)
2581 *new*	(6^-)	1527	(7^-)	1054.9(1)			0.368(28)
		1464	(5^-)	1118.4(1)			0.193(16)
		1209	6^-	1372.8(1)			0.126(11)
		551	6^-	2028.3(1)			0.121(11)
		434	7^-	2147.8(1)			0.192(19)
2607 *new*	(4^+)	993	3^+	1613.3(2)			1.0
2696 *new*	(3^+)	1524	4^+	1172.5(2)			0.465(42)
		993	3^+	1701.9(1)			0.535(49)
2726 *new*	[b]	993	3^+	1731.3(3)			0.529(65)
		503	4^-	2223.8(7)			0.471(72)
2730 *new*	[b]	1707	$5(^+)$	1023.9(2)			0.197(20)
		1464	(5^-)	1265.6(2)			0.210(24)
		551	6^-	2180.2(2)			0.593(56)
2765	(4^-)	1524	4^+	1241.7(2)			0.089(8)
		1248	(4^-)	1517.1(4)			0.011(2)
		993	3^+	1771.5(1)			0.079(8)
		503	4^-	2262.5(1)		$\Delta J = 0$	0.473(38)
		439	5^-	2325.7(1)			0.174(14)
		348	3^-	2416.9(1)			0.174(15)
2780 *new*	(5^+)	1777	6^+	1003.3(1)			0.073(6)
		1524	4^+	1256.2(1)			0.140(12)
		551	6^-	2229.4(1)			0.212(18)
		439	5^-	2340.3(1)			0.575(48)
2807 *new*	[b]	993	3^+	1812.6(1)			0.704(66)
		439	5^-	2367.3(2)			0.296(33)
2850 *new*	(3^-)	503	4^-	2346.6(1)			1.0
2883 *new*	[b]	1777	6^+	1106.2(1)			0.272(25)
		1524	4^+	1359.2(2)			0.293(27)
		551	6^-	2332.4(1)			0.436(39)
2910	(6^+)	2607	[b]	302.4(2)			0.125(70)
		551	6^-	2359.0(2)			0.558(63)
		439	5^-	2471.7(3)			0.317(36)
2962 *new*	(3^-)	503	4^-	2458.3(2)			0.400(51)
		348	3^-	2615.0(1)			0.600(65)
2979 *new*	[b]	1175	(2^-)	1803.9(2)			0.134(18)
		993	3^+	1984.8(2)			0.157(17)
		439	5^-	2539.8(2)			0.326(30)
		348	3^-	2631.0(1)			0.384(35)
2996[c] *new*	(5^+)	503	4^-	2492.3(8)			1.0
3023[c] *new*	[b]	320	2^-	2703.4(5)			1.0
3047[c] *new*	[b]	439	5^-	2607.5(6)			1.0
3097[c] *new*	[b]	348	3^-	2748.8(4)			1.0
3120 *new*	[b]	503	4^-	2617.4(2)			0.646(64)
		348	3^-	2772.1(2)			0.354(39)
3140	(6^-)	551	6^-	2589.3(2)			0.403(65)

TABLE I. (*Continued.*)

E_i (keV)	J_i^π	E_f (keV)	J_f^π	E_γ (keV)	$\alpha\,(M\lambda, E\lambda)$	Multipolarity	BR_γ
		439	5^-	2698.8(6)			0.218(28)
		434	7^-	2706.6(2)			0.379(44)
3182	(4^-)	503	4^-	2678.8(1)			0.446(57)
		439	5^-	2742.2(1)			0.485(50)
		348	3^-	2834.2(4)			0.069(10)
3236 *new*	(5^-)	1209	6^-	2026.6(3)			0.405(55)
		439	5^-	2797.3(2)			0.595(102)
3244	(7^-)	1464	(5^-)	1780.7(3)			0.128(14)
		1336	(5^-)	1908.3(2)			0.088(9)
		1209	6^-	2034.7(3)			0.018(6)
		551	6^-	2693.6(1)			0.332(35)
		439	5^-	2804.9(5)			0.297(44)
		434	7^-	2810.7(5)			0.137(32)
3260[c] *new*	(3^-)	993	3^+	2265.9(2)			1.0
3319[c] *new*	(4^-)	439	5^-	2879.1(5)			1.0
3326 *new*	(4^-)	503	4^-	2822.9(2)			0.615(72)
		439	5^-	2886.1(2)			0.385(48)
3394 *new*	(6^-)	1527	(7^-)	1867.0(1)			0.139(12)
		1209	6^-	2185.6(2)			0.056(6)
		916	8^-	2478.2(4)			0.029(8)
		583	8^-	2811.3(1)			0.297(25)
		551	6^-	2844.0(2)			0.078(9)
		434	7^-	2960.9(1)			0.400(34)
3444 *new*	(3^-)	1904	(3+)	1540.4(2)			0.373(51)
		1524	4^+	1920.7(2)			0.180(36)
		1248	(4^-)	2196.9(4)[c]			0.197(47)
		993	3^+	2449.6(4)			0.250(38)
3530[c] *new*	(5^-)	439	5^-	3090.9(5)			1.0
3662 *new*	(4^+)	1464	(5^-)	2198.3(3)[c]			0.159(26)
		1248	(4^-)	2413.3(2)			0.648(78)
		993	3^+	2668.3(4)			0.193(27)
3692 *new*	(6^-)	1527	(7^-)	2165.0(3)			0.412(94)
		434	7^-	3258.0(3)			0.588(151)
3879 *new*	(4^-)	503	4^-	3375.6(4)			0.257(36)
		439	5^-	3439.6(2)			0.444(54)
		348	3^-	3530.7(2)			0.299(43)
3900 *new*	(3^-)	1248	(4^-)	2651.3(2)			0.363(36)
		348	3^-	3551.7(1)			0.637(65)
4221 *new*	(5^-)	1777	6^+	2444.4(4)			0.068(11)
		1248	(4^-)	2973.1(2)			0.203(19)
		1209	6^-	3012.3(2)			0.164(17)
		434	7^-	3786.6(4)			0.251(27)
		348	3^-	3873.0(1)			0.314(29)
4605	$4^-, 5^-$	4221	(5^-)	384.4(2)			
		3900	(3^-)	705.2(1)			
		3879	(4^-)	726.7(2)			
		3692	(6^-)	912.8(2)			
		3662	(4^+)	943.9(1)			
		3530[c]	(5^-)	1074.6(2)[c]			
		3444	3^-	1160.8(2)			
		3394	6^-	1211.1(2)			
		3326	4^-	1279.6(2)			
		3319[c]	(4^-)	1286.5(1)[c]			
		3260[c]	(3^-)	1345.2(1)[c]			
		3244	(7^-)	1361.0(1)			
		3236	(5^-)	1367.8(2)			
		3182	(4^-)	1423.3(1)			

TABLE I. (*Continued.*)

E_i (keV)	J_i^π	E_f (keV)	J_f^π	E_γ (keV)	$\alpha\,(M\lambda, E\lambda)$	Multipolarity	BR_γ
		3140	(6^-)	1464.7(1)			
		3120	[b]	1484.7(2)			
		3097[c]	[b]	1507.6(2)[c]			
		3047[c]	[b]	1557.8(3)[c]			
		3023[c]	[b]	1581.5(2)[c]			
		2996[c]	[b]	1609.0(2)[c]			
		2979	(5^+)	1625.9(2)			
		2962	(3^-)	1641.8(1)			
		2910	(6^+)	1696.7(2)			
		2883	[b]	1722.3(1)			
		2850	(3^-)	1755.1(1)			
		2807	[b]	1798.5(1)			
		2780	(5^+)	1825.3(1)			
		2765	(4^-)	1839.8(1)			
		2730	[b]	1874.3(1)			
		2726	[b]	1879.4(2)			
		2696	(3^+)	1909.3(1)			
		2607	(4^+)	1997.4(3)			
		2581	(6^-)	2023.4(1)			
		2556	[b]	2048.9(2)			
		2525	(4^-)	2080.3(2)			
		2315	(4^+)	2290.1(2)			
		2177	(4^-)	2427.8(2)			
		2147	(5)	2458.9(2)			
		2109	(6^-)	2496.5(1)			
		2100	$5(^+)$	2505.4(1)		$E1(+M2)$	
		2081	(4^-)	2524.0(4)			
		2034	(5^-)	2570.9(2)		$M1(+E2)$	
		2007	$4(^+)$	2598.6(1)			
		1981	7^-	2624.4(1)		$E2$	
		1777	6^+	2828.9(2)		$E1(+M2)$	
		1707	$5(^+)$	2898.7(2)			
		1527	(7^-)	3078.3(3)			
		1524	4^+	3081.2(1)		$E1(+M2)$	
		1464	(5^-)	3142.2(1)			
		1390	(4^-)	3214.8(1)			
		1374	(3^-)	3231.0(1)			
		1336	(5^-)	3269.3(1)			
		1248	4^-	3357.0(1)			
		1209	6^-	3396.5(1)		$\Delta J = 1$	
		1197	(1,2)	3407.6(1)			
		1175	(2^-)	3429.6(2)			
		993	3^+	3611.1(2)			
		972	2^-	3633.1(1)		$E2$	
		551	6^-	4054.8(1)			
		503	4^-	4101.6(3)		$M1(+E2)$	
		439	5^-	4165.6(1)			
		434	7^-	4171.4(1)			
		348	3^-	4256.9(1)		$E2$	
		320	2^-	4285.1(2)			

[a]α-decaying isomer, $T_{1/2} = 3.04 \times 10^6$ y.
[b]The spin-parity value could not be assigned.
[c]Tentative placement.
[d]Transition energy calculated from level energy difference.
[e]γ-ray intensity calculated assuming theoretical conversion coefficient.

All information on the observed transitions is summarized in Table I. For example, the lines 318, 611, and 944 keV feeding the states at 1209, 916, and 589 keV, respectively, established the excitation at 1527 keV. This state is populated by the primary γ ray of 3078 keV and two secondary transitions: 1055 and 1867 keV from states at 2581 and 3394 keV, newly observed as well. This is the lowest from newly found excitations in ^{210}Bi and one of the two such states discovered below the excitation energy of 2 MeV. The second is the state at 1904 keV decaying by two γ rays, i.e., 910 and 1584 keV, to the states known previously at 993 and 320 keV. It is populated by the 103-keV transition from the 2007-keV level, unobserved owing to the large conversion for such low-energy line (the conversion coefficient is equal to 9.36, assuming $M1$ multipolarity; see Table I), as well as by the 1540-keV γ ray from the 3444-keV state. Higher, in the energy range of 2.5–4.2 MeV, the newly found states make up the majority. A few of them, i.e., excitations at 2996-, 3023-, 3047-, 3097-, 3260-, 3319-, and 3530-keV are populated by one primary γ ray and deexcited also by only one transition. This means that it is not possible to define the order of the γ rays in these cases; therefore, the energy of the state could be only tentatively established. Such levels were marked by the dashed lines in Figs. 3–6 and 9.

The energies of some low-energy lines, which are strongly converted, were calculated from the energies of the states.

Strong peaks coming from contaminating isotopes, ^{28}Al and ^{36}Cl, with high cross section for thermal neutron capture, were identified as well [14]. Moreover, the first escape peaks of the intense high-energy γ rays from ^{210}Bi were also observed. Some of them are indicated in Fig. 1.

The investigations made it possible to establish 64 branches of the decay from the neutron capture state, of which 40 are newly observed or were observed prior to this study but not assigned as primary γ rays. They are marked in red in Fig. 3. Thirty-three new states populated mainly by primary γ rays were also located in the energy range of 1527–4221 keV. The energy of the capture state was calculated from the sums of γ-ray energies belonging to strong cascades. The value resulting from this analysis is 4605.2(1) keV.

Owing to the large self-absorption of γ rays in the target (3 g) the detection efficiency ε_γ had to be corrected with respect to the original evaluation [9]. This correction was based on the intensity balance of γ rays in strong cascades. For the lines with energy $E > 650$ keV the effect of self-absorption was not observed (it was checked for the 674- and 1065-keV lines); therefore, the new efficiency curve was obtained under the assumption that in the high-energy region ($E > 800$ keV) the efficiency curve overlaps with the one evaluated originally [9]. The same function was used,

$$\varepsilon_\gamma(E) = \exp\left\{a_1 - [a_2 + a_3\exp(-a_4 E)]\exp(-a_5 E)\ln\frac{E}{E_0}\right\}, \quad (1)$$

and the new parameters are $a_1 = 6.85(41)$, $a_2 = 0.471(61)$, $a_3 = 1.36(14)$, $a_4 = 0.00954(77)$ keV^{-1}, and $a_5 = -2.67(75) \times 10^{-5}$ keV^{-1}; the E_0 value was set to 0, as in Ref. [9]. The results are shown in Fig. 7.

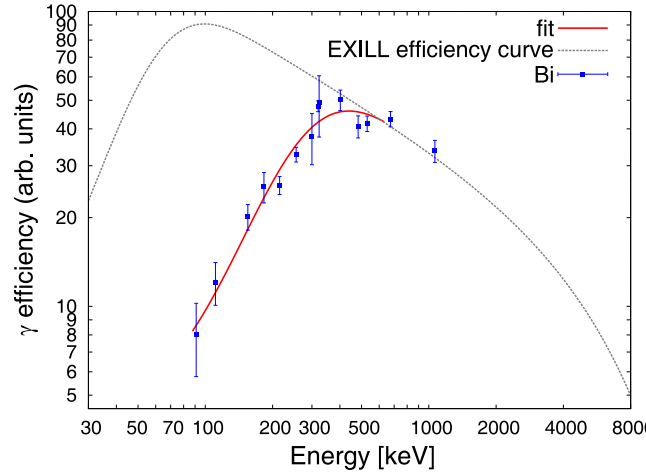

FIG. 7. Corrected relative full-energy-peak γ efficiency of the EXILL array for the neutron capture experiment on a 3-g-thick ^{209}Bi target (in red) compared to the curve from Ref. [9], obtained for thinner targets. See text for further explanations.

Based on the corrected efficiency, the γ-branching ratios were calculated. Gates were set on transitions above the observed level and relative intensity ratios of the deexciting transitions (defined as a ratio of the intensity of the γ transition to the summed intensity of all transitions deexciting the state of interest, corrected for the internal conversion) were extracted. In case of some low-energy lines, which were not clearly visible owing to the larger background or some contaminations, the proper ratio was calculated based on the intensities of the transitions following the decay. For example, in the case of the 28-keV line deexciting the 348-keV level to the 320-keV state, the intensity was calculated based on the intensity of the observed 320-keV line. One should note that the conversion coefficients used for low-energy transitions were not extracted from the data but calculated for the lowest possible order of multipole for a given γ ray (column 6 of Table I).

B. Angular correlations, multipolarity determinations, and spin-parity assignments

Information on the multipolarities of γ transitions known in ^{210}Bi is rather limited. In the present work, the γ-γ coincidence data made it possible to perform a detailed analysis of angular correlations for a large number of cases, following the formalism of Refs. [15,16]. The angular correlation function is expressed as a sum of Legendre polynomials, $P_n(\cos\theta)$, parametrized by coefficients A_2 and A_4,

$$W(\theta) = A_0[1 + A_2 P_2(\cos\theta) + A_4 P_4(\cos\theta)], \quad (2)$$

where A_n are the products of two coefficients, $A_n(1)$ and $A_n(2)$, depending on the character of two considered transitions:

$$A_n = q_n A_n(1) A_n(2), \quad \text{with } n = 2,4. \quad (3)$$

q_n are attenuation coefficients associated with the finite solid angle of the detectors (geometry and size of the crystal, distance from the radiation source) and may be

TABLE II. The measured angular-correlations coefficients A_2 and A_4, assigned multipolarities, and the theoretical A_2^{theor} and A_4^{theor} values, calculated by using the extracted mixing ratios, are presented for each pair of $E_{\gamma 1}$-$E_{\gamma 2}$ transitions.

$E_{\gamma 1}$-$E_{\gamma 2}$	Multipolarity	A_2	A_4	A_2^{theor}	A_4^{theor}	δ_1	δ_2
393-320	$\Delta J = 0$-$M1(+E2)$	−0.22(6)	0.02(11)	−0.14	0.00	−0.01(32)	0.05(3)
393-674	$\Delta J = 0$-$E1(+M2)$	−0.12(4)	0.07(9)	−0.14	0.00	−0.01(32)	0.02(3)
393-1204	$\Delta J = 0$-$E1(+M2)$	−0.10(4)	−0.08(7)	−0.16	0.00	−0.01(32)	−0.04(6)
409-563	$M1$-$M1(+E2)$	−0.05(4)	−0.02(8)	−0.05	0.00	0.00[a]	0.18(16)
530-320	$M1(+E2)$-$M1(+E2)$	0.01(1)	−0.03(3)	0.01	0.00	0.08(2)	0.05(3)
530-674	$M1(+E2)$-$E1(+M2)$	0.02(1)	−0.02(2)	0.01	0.00	0.08(2)	0.02(3)
611-645	$(M1)$-$(M1)$	0.07(5)	0.07(11)	0.05	0.00	0.00[a]	0.00[a]
634-563	$\Delta J = 1$-$M1(+E2)$	−0.07(6)	−0.05(12)	−0.05	0.00	0.00[a]	0.18(16)
674-320	$E1(+M2)$-$M1(+E2)$	0.03(1)	−0.01(2)	0.03	0.00	0.02(3)	0.05(3)
809-320	$M1(+E2)$-$M1(+E2)$	0.07(2)	−0.04(4)	0.07	0.00	−0.04(3)	0.05(3)
951-320	$M1(+E2)$-$M1(+E2)$	0.22(9)	−0.03(20)	0.22	0.00	0.22(23)	0.05(3)
1013-320	$(M1 + E2)$-$M1(+E2)$	0.10(5)	0.01(11)	0.10	0.00	−0.12(10)	0.05(3)
1013-674	$(M1 + E2)$-$E1(+M2)$	0.10(2)	0.01(4)	0.10	0.00	−0.12(10)	0.02(3)
1175-320	$(E1)$-$M1(+E2)$	0.04(3)	0.03(6)	0.04	0.00	0.02(6)	0.05(3)
1204-320	$E1(+M2)$-$M1(+E2)$	0.07(3)	−0.01(7)	0.07	0.00	−0.04(6)	0.05(3)
1337-320	$E1(+M2)$-$M1(+E2)$	0.05(3)	−0.02(7)	0.05	0.00	0.02(6)	0.05(3)
1398-311	$M1(+E2)$-$M1(+E2)$	0.09(5)	−0.01(10)	0.09	0.00	0.05(5)	0.04(8)
1596-320	$\Delta J = 1$-$M1(+E2)$	0.05	−0.08(15)	0.05	0.00	0.00(10)	0.05(3)
1659-320	$E1(+M2)$-$M1(+E2)$	−0.06(5)	−0.08(10)	−0.06	0.00	0.24(15)	0.05(3)
1825-320	$\Delta J = 0$-$M1(+E2)$	−0.10(4)	0.02(9)	−0.10	0.00	0.21(17)	0.05(3)
2263-320	$\Delta J = 0$-$M1(+E2)$	−0.14(6)	0.07(12)	−0.15	0.00		0.05(3)
2505-320	$E1(+M2)$-$M1(+E2)$	−0.14(2)	−0.03(3)	−0.14	0.00	0.02(13)	0.05(3)
2505-393	$E1(+M2)$-$\Delta J = 0$	0.24(3)	−0.01(6)	0.19	0.00	0.02(13)	−0.01(32)
2505-674	$E1(+M2)$-$E1(+M2)$	−0.13(2)	−0.02(5)	−0.13	0.00	0.02(13)	0.02(3)
2505-1596	$E1(+M2)$-$\Delta J = 1$	−0.11(2)	0.03(4)	−0.13	0.00	0.02(13)	0.00(10)
2571-320	$M1(+E2)$-$M1(+E2)$	0.06(6)	0.00(12)	0.06	0.00	−0.06(9)	0.05(3)
2571-1485	$M1(+E2)$-$M1(+E2)$	0.11(6)	0.01(12)	0.11	0.00	−0.06(9)	$0.3(^{+4}_{-2})$
2624-1065	$E2$-$M1(+E2)$	−0.13(7)	−0.10(14)	−0.13	0.00	0.0[a]	0.10(12)
2624-1398	$E2$-$M1(+E2)$	−0.10(3)	0.02(7)	−0.10	0.00	0.0[a]	0.05(5)
2624-1430	$E2$-$M1(+E2)$	−0.19(3)	0.00(7)	−0.19	0.00	0.0[a]	0.45(21)
2624-1709	$E2$-$E2$	0.11(3)	0.04(5)	0.10	0.01	0.0[a]	0.0[a]
2829-1337	$E1(+M2)$-$E1(+M2)$	0.10(2)	0.04(4)	0.10	0.00	0.06(4)	0.02(6)
3081-320	$E1(+M2)$-$M1(+E2)$	0.07(2)	0.03(4)	0.07	0.00	−0.04(5)	0.05(3)
3081-674	$E1(+M2)$-$E1(+M2)$	0.07(2)	−0.01(5)	0.07	0.00	−0.04(5)	0.02(3)
3397-320	$\Delta J = 1$-$M1(+E2)$	0.16(8)	−0.04(19)	0.16	0.00	0.11(17)	0.05(3)
3397-769	$\Delta J = 1$-$M1(+E2)$	0.15(7)	0.07(15)	0.15	0.00	0.11(17)	−0.02(8)
3397-775	$\Delta J = 1$-$M1(+E2)$	0.09(5)	−0.04(11)	0.09	0.00	0.11(17)	0.01(7)
3633-409	$E2$-$M1$	−0.08(3)	0.04(5)	−0.08	0.00	0.00[a]	0.00[a]
3633-563	$E2$-$M1(+E2)$	0.10(3)	0.03(6)	0.12	0.00	0.00[a]	0.18(16)
4102-320	$M1(+E2)$-$M1(+E2)$	0.10(1)	0.00(2)	0.10	0.00	−0.10(2)	0.05(3)
4102-348	$M1(+E2)$-$E2$	−0.20(7)	0.03(13)	−0.15	0.00	−0.10(2)	0.00[a]
4257-320	$E2$-$M1(+E2)$	−0.05(2)	0.04(3)	−0.07	0.00	0.00[a]	0.05(3)

[a]The mixing ratio $\delta = 0$ was deduced from the decay pattern.

calculated from theory or extracted from experimental data.

In the analysis of the angular correlations, the detectors were divided into groups depending on the relative angle between them. As the detectors of EXOGAM used in the experiment were placed in one ring in octagonal geometry, the double γ-coincidence data could be sorted into three matrices corresponding to average angles between detectors of 0° (in practice 180°), 45° (and 135°), and 90°. The number of counts in a given coincidence peak obtained by gating on a particular matrix was normalized depending on the number of detector pairs available in each of the three groups (4, 16, and 8 for the angles 0°, 45°, and 90°, respectively). The attenuation coefficients q_n were determined by using cascades from ^{60}Co and ^{152}Eu sources with well-defined anisotropies. This resulted in $q_2 = 0.86(2)$ and $q_4 = 0.60(3)$ [9].

Table II summarizes the results of the angular correlations studies: For each combination of $E_{\gamma 1}$, $E_{\gamma 2}$ transitions, assigned multipolarities of the transitions, experimental A_2 and A_4 angular correlation coefficients and δ_1 and δ_2 mixing

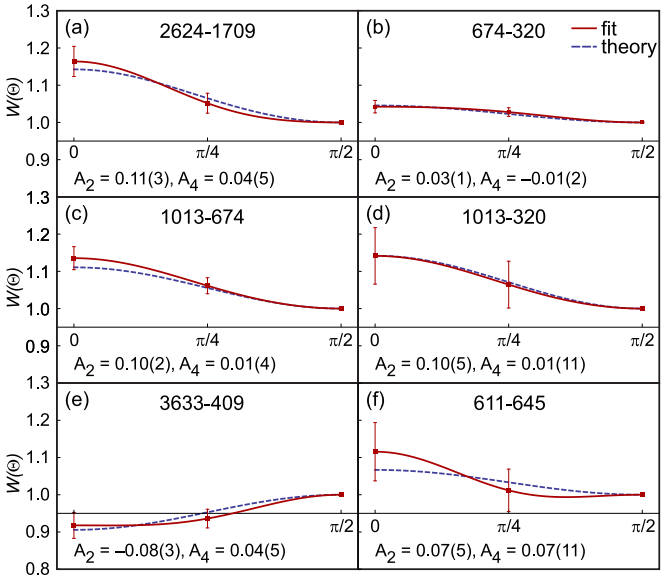

FIG. 8. Selected examples of angular correlations of γ rays from ^{210}Bi. The A_2 and A_4 values are experimental coefficients of the fitted functions.

ratios are given. In addition, A_2^{theor} and A_4^{theor} theoretical angular correlation coefficients calculated by using assigned multipolarities and extracted mixing ratios are shown. These results are discussed in more detail in the following part, for selected cases. At first, the method was tested on known transitions in ^{210}Bi which are considered very pure and with rather well-established multipolarities and mixing ratios. This is important to validate the method for further investigation. Later, the angular correlation for other strong transitions were studied to extract information about their multipolarities.

1. 1981-keV level: $J^\pi = 7^-$ spin confirmation

A good example for testing the angular correlation method is the cascade 2624-1709 keV [see Fig. 8(a)], consisting of a primary γ ray which populates the intermediate state at 1981 keV and a second γ ray feeding the long-lived isomer at 271 keV. The latter transition, reported to be of pure $E2$ character [7], deexcites the state with $J^\pi = (7^-)$; therefore, the former γ ray should come from the 5^- capture state (as $4^- \rightarrow 7^-$ $M3$ transition would be very slow) and have $E2$ multipolarity as well. The coefficients of the fitted function are $A_2 = 0.11(3)$, $A_4 = 0.04(5)$, while the theoretical values for $E2$-$E2$ cascade proceeding through the states with spins $5 \rightarrow 7 \rightarrow 9$ are $A_2 = 0.10$ and $A_4 = 0.01$. From this one can conclude that the considered cascade should consist of two quadrupole transitions, what confirms the $J^\pi = 7^-$ value for the 1981-keV state. The 2624-keV line was then used to extract the mixing ratios for three transitions deexciting the 1981-keV level, i.e., 1430-, 1398-, and 1065-keV γ rays. The constructed correlation functions allowed to establish the $M1$ character for those lines with possible small admixtures of $E2$ multipolarity (Table II). In addition, the correlation of the 1398-311-keV pair made it possible to extract $\delta = 0.04(8)$ for the 311-keV line. This means that the 311-keV γ ray is of pure or almost pure $M1$ character.

2. 993-keV level: $J^\pi = 3^+$ spin confirmation

The 674- and 320-keV γ rays, belonging to the strongest cascade leading to the ground state, depopulate the level at 993 keV and do not have firmly established multipolarities. The latter one is a $2^- \rightarrow 1^-$ transition considered as a pure $M1$ [7], while the 674-keV line, $3^+ \rightarrow 2^-$, is expected to be of pure $E1$ character. The coefficients of the correlation function for those two transitions, $A_2 = 0.03(1)$ and $A_4 = -0.01(2)$, are very close to the theoretical values for a pure $E1$-$M1$ cascade: 0.05 and 0.00, respectively [see Fig. 8(b)]. To extract the possible mixing ratios for the 674- and 320-keV γ rays, the correlation functions with the 1013-, 2505-, and 3081-keV lines (each of which is in coincidence with the 674-320-keV cascade) were analyzed. This investigation resulted in the values of δ reported in Table II and confirmed the $J^\pi = 3^+$ value for the 993-keV level. Since the analysis of the angular correlations for the 320-keV γ ray is crucial for defining precisely the admixture of $E2$ multipole in this transition, which is important also for the applications in reactor science, a dedicated investigation has been performed and it will be reported in a separate publication on this issue [17].

3. 4605-keV level: Capture state

An important part of the angular correlations analysis carried out in this work aimed at establishing the spin-parity value of the neutron capture state in ^{210}Bi. To this end, during the data analysis we considered the following combinations of γ rays: 4257-320, 4102-320, 4102-348, 2829-1337, and 3633-409 keV. At first, an angular correlation function was constructed for the pair of transitions 4257-320 keV, in which the first one is a primary γ ray feeding the 3^- state at 348 keV. The cascade goes through the intermediate, highly converted, and thus unobserved, 28-keV transition, which most probably is of $M1$ character. Assuming the mixing ratio $M1(+E2)$ established in the analysis for the 320-keV γ ray, the multipolarity of the 4257-keV transition could be extracted, yielding $A_2 = -0.05(2)$ and $A_4 = 0.04(3)$. This indicates its $\Delta J = 2$ nature and suggests the $J^\pi = 5^-$ value for the neutron capture state.

The multipolarity of the 4102-keV transition, a primary γ ray feeding the 4^- state at 503 keV, was deduced as $M1(+E2)$ from the correlation analysis with the 320-keV γ ray, with $\delta = -0.10(2)$. These transitions are connected by the 155-28-keV cascade of which only the 155-keV γ ray is observed. Also, the analysis of the same 4102-keV line in coincidence with the stretched $E2$ 348-keV transition (the cascade goes through the intermediate 155-keV line), feeding the ground state from level 3^-, pointed to its $\Delta J = 1$ character. As these observations are consistent with an $M1$ multipolarity for the 4102-keV γ ray, the $J^\pi = 5^-$ assignment for the neutron capture state was proposed.

Further support for this scenario comes from the analysis of multipolarity of the 2829-keV primary transition, feeding the 6^+ state. By investigating the 2829-1337-keV cascade in which the second transition is likely of pure $E1$ nature

(confirmed by the 1337-320 keV correlation analysis), a $\Delta J = 1$ character of the 2829-keV line was concluded. This result is again in line with a $J^\pi = 5^-$ spin-parity assignment for the neutron capture state.

As shown in the previous paragraphs, the multipolarity of three strong primary γ rays in ^{210}Bi was determined from the angular correlation analysis. They all imply the 5^- quantum numbers for the capture state. However, one should notice that some primary γ rays, e.g., 4285, 3633, 3430 keV, feed the 2^- states. This contradicts the $J^\pi = 5^-$ assignment for the capture state, because $M3$ transitions would be very delayed. To elucidate this issue, the correlation function of the 409-keV, $2^- \rightarrow 1^-$ transition (established to be of pure $M1$ character) and the 3633-keV primary γ ray (leading to the 2^- state) was investigated. The analysis yielded coefficient values $A_2 = -0.08(3)$ and $A_4 = 0.04(5)$, shown in Fig. 8(e), which suggest a $\Delta J = 2$ value for the 3633-keV primary transition. Since there is no parity change in this case, the only possibility is an $E2$ character for the 3633-keV line. As a consequence, the J^π value for the capture state would be 4^-. This demonstrates that the cold neutron capture process on ^{209}Bi populates states with spin-parity values of 4^- and 5^-, which is in line with the expectations: the coupling of the capture neutron spin, 1/2 $\hbar$, to the ^{209}Bi ground state spin, 9/2 $\hbar$, may result in the 4^- and 5^- spin values. One may then conclude that at least two states having spin-parity values 4^- or 5^- can contribute to the capture level populated in the ^{209}Bi$(n,\gamma)^{210}$Bi reaction. The composition of the capture state could be studied in detail by using the technique based on polarized neutrons and oriented target nuclei, as it was done for ^{59}Co, reported in Ref. [18].

4. 1524-keV level: $J^\pi = 4^+$ spin confirmation

The intense transition of 530 keV [Fig. 1(b)], which was found to deexcite the (4^+) state at 1524 keV, was investigated in correlations with the 320- and 674-keV lines. Assuming small mixing ratios for those γ rays, the mixing ratio for the 530-keV transition was calculated from the coefficients of two correlation functions. The average result is 0.08(2). The second solution, $\delta = 5.3(6)$ is less likely. The 1175-keV line, parallel to the 530-keV transition and also deexciting the 1524-keV level, was also examined in correlation with the 320-keV transition. An $E1$ character was deduced for the 1175-keV line [a small mixing of 0.02(6) is not excluded]. The primary γ ray which feeds the 1524-keV state—3081 keV—was examined in correlations with the 320- and 674-keV lines. The coefficients of the fitted functions (Table II) point to its $\Delta J = 1$ character (with small mixing ratio) and suggest a $5^- \rightarrow 4$ decay. All these results confirm the 4^+ spin-parity value for the state at 1524 keV.

5. 1209-keV level: $J^\pi = 6^-$ spin confirmation

The two strongest transitions deexciting the state at 1209 keV, i.e., 775- and 769-keV γ rays, which feed the 7^- and 5^- states, respectively, were examined in correlation with the primary γ ray of 3397 keV. The latter is of $\Delta J = 1$ character, as follows from the angular correlation analysis with the 320-keV line [$\delta = 0.11(17)$]. In turn, the angular correlation functions for the 3397-775- and 3397-769-keV pairs are in line with a $\Delta J = 1$ nature of both 775- and 769-keV transitions, which are probably of $M1$ multipolarity. Therefore, one can confirm the previous $J^\pi = 6^-$ assignment for the 1209-keV level.

6. 1248-keV level: $J^\pi = 4^-$ spin confirmation

The angular correlation function of the 809-320-keV cascade, together with the mixing ratio $\delta = -0.04(3)$ of the 809-keV transition, points to the $\Delta J = 1$ nature of the 809-keV γ ray which deexcites the 1248-keV level and populates a 5^- state. This agrees with the (4^-) assignment to the 1248-keV level. Concerning the 3357-keV primary γ ray, feeding the 1248-keV level, it is not possible to state, firmly, which level it deexcites: 4^- or 5^-, because the correlation function for the 3357-320-keV pair is not unambiguous.

7. 1707-keV level: $J^\pi = 5^{(+)}$ spin confirmation

The line 1204 keV deexcites the state at 1707 keV, for which the (5^+) spin-parity was previously assigned. Then, the multipolarity of this line should be $E1$, as it feeds a 4^- state. To check this, the correlation with the 320-keV line was considered. The $A_2 = 0.07(3)$ and $A_4 = -0.01(7)$ extracted values are in good agreement with the theoretical ones for pure $E1$-$M1$ cascade (0.07 and 0.00). However, taking into account the possible small mixing ratio of the 320-keV line, one cannot exclude a small admixture of higher multipole for the 1204-keV transition ($\delta = -0.04$).

8. 2007-keV level: $J^\pi = 4^{(+)}$ spin confirmation

Two transitions deexciting the state at 2007 keV, the 1013- and 1659-keV γ rays, were intense enough to perform the analysis of their angular correlations with the 320- and 674-keV line. The 2007-keV state has previously assigned a tentative $J^\pi = 4^+$. Both transitions exhibit some mixing, as it is seen from the analysis of pairs: 1013-320 [see Fig. 8(c)], 1013-674 [see Fig. 8(d)], and 1659-320 keV (see Table II). As a result, the $M1 + E2$ and $E1+(M2)$ multipolarities were proposed for the 1013- and 1659-keV transitions, respectively. This is in agreement with a $J = 4$ assignment for the 2007-keV level.

9. 1197-keV level: $J = (1,2)$ spin assignment

Concerning the transitions from newly found states, they are usually too weak to perform analysis of the angular correlations. An example of those for which it was possible is the 634-keV line deexciting the 1197-keV state. The angular correlation function for the 634-563-keV pair of γ rays was considered. The latter is the $1^- \rightarrow 1^-$ $M1(+E2)$ transition, for which a mixing ratio of of 0.18(16) was extracted from the correlation with the lines 409 keV ($M1$) and 3633 keV ($E2$). Then, the coefficients of the angular correlation function for the 634-563-keV pair, i.e., $A_2 = -0.07(6)$ and $A_4 = -0.05(12)$, suggest the $\Delta J = 1$ character of the 634-keV transition, as $\Delta J = 0$ and $\Delta J = 2$ possibilities would result in positive sign of A_2 coefficient. Because the 634-keV γ ray, depopulating the 1197-keV state, feeds directly the 1^- state, a spin value of 2 can be assigned to the 1197-keV level (however, the $J = 1$ assignment cannot be totally excluded). This is in agreement with the observed paths of the decay, to 3^- and 1^- levels (Table I).

10. 1527-keV level: $J^\pi = (7^-)$ spin assignment

From the newly found transitions deexciting the new state at 1527 keV, only the 611-keV line was intense enough to perform the analysis of angular correlations. The 611-645-keV pair was investigated [Fig. 8(f)]. The latter is an $8^- \rightarrow 9^-$ transition, which suggests its $M1$ character (since the extraction of the mixing ratio was not possible, a pure $M1$ multipolarity is assumed in the current analysis). The coefficients $A_2 = 0.07(5)$ and $A_4 = 0.07(11)$ are, within the errors, in agreement with the assumption of pure $\Delta J = 1 - M1$ cascade (Table II). As a consequence, the 611-keV line from the 1527-keV state is compatible with a $\Delta J = 1$ character; this suggests the spin value of 7 for the 1527-keV level. Moreover, the negative parity of this state may be deduced from the fact that the primary γ ray feeding it should be most likely of $E2$ character ($5^- \rightarrow 7^-$).

11. 1390-keV level: $J^\pi = (4^-)$ spin confirmation

The angular correlation function for the 951-keV transition, deexciting the 1390-keV level, and the 320-keV line determined the $\Delta J = 1$ character of the 951-keV γ ray. In addition, the mixing ratio $\delta = 0.22(23)$ suggests a $M1(+E2)$ multipolarity and confirms the tentative (4^-) spin-parity value for the 1390-keV state.

12. 2034-keV level: $J^\pi = (5^-)$ spin confirmation

The correlation function for the 2571-1484-keV pair (being the former a primary γ ray leading to the 2034-keV state) provides a positive $A_2 = 0.11(6)$ value, which suggests $4^- \rightarrow 5 \rightarrow 6^-$ or $4^- \rightarrow 4 \rightarrow 6^-$ scenarios for this cascade. In turn, the correlation of the 2571-320-keV pair points to a $\Delta J = 1$ nature of the primary γ ray, with possible small admixture of higher multipole: $\delta = -0.06(9)$. One should note that the errors are large in this case: $A_2 = 0.06(6)$ and $A_4 = 0.00(12)$. Eventually, the $M1$ multipolarities are proposed for both 2571- and 1484-keV transitions. The mixing ratio for the 1484-keV γ ray was also extracted: $\delta = 0.3(^{+4}_{-2})$. These observations are in agreement with the $J^\pi = (5^-)$ value, previously assigned to the 2034-keV level.

13. 2100-keV level: $J^\pi = 5(^+)$ spin confirmation

The two lines deexciting the 2100-keV level, i.e., 393 and 1596 keV, were investigated. The angular correlations for the 393-320-, 393-674-, and 393-1204-keV pairs suggest a $\Delta J = 0$ nature of the 393-keV γ ray ($5 \rightarrow 5^+$) with calculated average $\delta = 0.01(32)$. The second transition, 1596 keV, leading to a 4^- state at 503 keV, was investigated in correlation with the 320-keV line. The A_2 and A_4 coefficients point to two possibilities: $5 \rightarrow 4^-$ or $4 \rightarrow 4^-$. However, the correlations of the primary γ ray leading to the 2100-keV level, i.e., the 2505-keV line, with the 393- and 1596-keV transitions, support the scenario of $5^- \rightarrow 5 \rightarrow 5^+$ for the 393- and $5^- \rightarrow 5 \rightarrow 4^-$ for the 1596-keV line. On this basis, one can assume that the 1596-keV transition is of $\Delta J = 1$ character and the 2505-keV γ ray of $\Delta J = 0$ nature.

The analysis involving the 2505-keV γ ray, discussed above, confirms this spin 5 assignment. Considering, in addition, the analysis of angular correlations involving the pairs of γ rays 2505-320 and 2505-674 keV, the $5(^+)$ assignment is preferred, although the $5(^-)$ possibility cannot be rigorously excluded.

14. 2765-keV level: $J^\pi = (4^-)$ new spin assignment

The 2263-keV line deexciting the 2765-keV level was investigated in correlation with the 320-keV transition. The coefficients $A_2 = -0.14(6)$ and $A_4 = 0.07(12)$ are in line with the scenario of a $4 \rightarrow 4^-$ transition. The state at 2765 keV was previously considered as a (3^+), but our result suggests rather a $J^\pi = (4^-)$ spin assignment. The δ mixing ratio for the 2263-keV transition was not extracted owing to its small value with large error.

15. 2780-keV level: $J^\pi = (5^+)$ spin assignment

The angular correlation function for the 1825-320-keV cascade with negative $A_2 = -0.10(4)$ value suggests a $5^- \rightarrow 5$ or a $4^- \rightarrow 6$ scenarios for the 1825-keV primary transition, feeding the 2780-keV level. In turn, the positive A_2 coefficient of the fitted function for the 1825-2340-keV cascade points to a $\Delta J = 0$ nature of both γ rays, $5^- \rightarrow 5 \rightarrow 5^-$ (in this case the statistics is too low to extract reliable information about δ). Assuming a $5^- \rightarrow 5$ scenario for the 1825-keV line, its $\delta = 0.21(17)$ was extracted from the coefficients of the 1825-320-keV correlation. On the basis of this analysis we propose a $J^\pi = (5^+)$ for the state at 2780 keV.

16. 1904-keV level: $J = (3^+)$ spin assignment

The γ rays feeding and deexciting the level at 1904 keV are too weak to investigate their angular correlations. However, because the spin-parity values of some of the states involved in this decay were confirmed in the analysis discussed above, one may try to deduce the spin value of the 1904-keV level with the help of observed decay pattern. This level is populated by the lines of energy 103 and 1540 keV from the states $4(^+)$ at 2007 keV and (3^-) at 3444 keV, respectively. In addition, it feeds the states 2^- at 320 keV and 3^+ at 993 keV, respectively. Therefore, the $J = (3^+)$ possibility is favored.

III. COMPARISON WITH SHELL-MODEL CALCULATIONS

In the course of the γ-coincidence analysis, 70 states were found to be populated following the decay of the neutron capture state in ^{210}Bi; 33 of them were not reported in the literature previously. Having such a rich set of experimental information, a detailed comparison with shell-model calculations could be made. The calculations were performed by the computer code OXBASH [19], using the residual interaction of Kuo and Herling [20] with modifications introduced by Warburton and Brown (KHPE [21]). In the following we discuss in detail a direct comparison between data and theory for states below 2 MeV and above 2 MeV excitation energy. Figure 9 shows a comparison between experimental results and theory; all the information is also reported in Table III.

FIG. 9. Comparison between the experimental results and shell-model calculations. (a) Level scheme between 0 and 2315 keV; (b) between 2525 and 4605 keV (capture state). In each panel: (i) left, levels observed in the present experiment (red, newly found; marked by closed star, observed, but without theoretical counterparts; marked by open star, new theoretical interpretation); (ii) middle, theoretical predictions from the shell-model calculations; (iii) right, experimental levels reported in previous experiments (NuDat database [3]), not observed in present data. See text for details.

TABLE III. List of shell-model states populated in ^{210}Bi after the neutron capture reaction. Spin-parity values, main configurations, and calculated energies are given in the first three columns and compared with experimental energies in the fourth column. The last column provides the probability of the main configuration.

J^π	Main configuration	Calc. energy (keV)	Exp. energy (keV)	Probability of the main configuration (%)
1_1^-	$\pi h_{9/2}\nu g_{9/2}$	0	0	95.93
0_1^-	$\pi h_{9/2}\nu g_{9/2}$	48	47	97.92
9_1^-	$\pi h_{9/2}\nu g_{9/2}$	272	271	99.11
2_1^-	$\pi h_{9/2}\nu g_{9/2}$	319	320	95.73
3_1^-	$\pi h_{9/2}\nu g_{9/2}$	347	348	97.25
7_1^-	$\pi h_{9/2}\nu g_{9/2}$	434	434	97.52
5_1^-	$\pi h_{9/2}\nu g_{9/2}$	441	439	97.78
4_1^-	$\pi h_{9/2}\nu g_{9/2}$	504	503	98.10
6_1^-	$\pi h_{9/2}\nu g_{9/2}$	550	551	98.64
1_2^-	$\pi h_{9/2}\nu i_{11/2}$	565	563	49.36
8_1^-	$\pi h_{9/2}\nu g_{9/2}$	584	583	97.39
8_2^-	$\pi f_{7/2}\nu g_{9/2}$	916	916	92.47
2_2^-	$\pi f_{7/2}\nu g_{9/2}$[a]	974	972	43.85
3_1^+	$\pi h_{9/2}\nu j_{15/2}$	993	993	94.03
2_3^-	$\pi h_{9/2}\nu i_{11/2}$[a]	1173	1175	52.00
			1197	
6_2^-	$\pi f_{7/2}\nu g_{9/2}$	1209	1209	93.79
4_2^-	$\pi f_{7/2}\nu g_{9/2}$[a]	1248	1248	92.19
5_2^-	$\pi h_{9/2}\nu i_{11/2}$	1335	1336	74.83
3_2^-	$\pi h_{9/2}\nu i_{11/2}$	1375	1374	93.70
4_3^-	$\pi h_{9/2}\nu i_{11/2}$[a]	1389	1390	96.12
5_3^-	$\pi f_{7/2}\nu g_{9/2}$	1464	1464	74.63
4_1^+	$\pi h_{9/2}\nu j_{15/2}$	1524	1524	91.72
			1527	
5_1^+	$\pi h_{9/2}\nu j_{15/2}$	1708	1707	93.21
6_1^+	$\pi h_{9/2}\nu j_{15/2}$	1776	1777	94.08
3_2^+	$\pi i_{13/2}\nu g_{9/2}$	1898	1904	94.44
7_4^-	$\pi h_{9/2}\nu d_{5/2}$	1981	1981	94.15
			2007	
5_4^-	$\pi h_{9/2}\nu d_{5/2}$	2090	2034	87.23
4_4^-	$\pi h_{9/2}\nu d_{5/2}$	2021	2081	60.98
5_2^+	$\pi i_{13/2}\nu g_{9/2}$[a]	2198	2100	93.07
6_4^-	$\pi h_{9/2}\nu d_{5/2}$	2168	2109	80.93
			2147	
4_5^-	$\pi f_{7/2}\nu i_{11/2}$	2199	2177	75.78
4_2^+	$\pi i_{13/2}\nu g_{9/2}$	2172	2315	96.68
4_6^-	$\pi h_{9/2}\nu s_{1/2}$	2548	2525	75.63
			2556	
6_6^-	$\pi f_{7/2}\nu d_{5/2}$	2633	2581	88.83
4_3^+	$\pi i_{13/2}\nu i_{11/2}$	2580	2607	56.44
3_3^+	$\pi i_{13/2}\nu i_{11/2}$	2709	2696	98.24
			2726	
			2730	
4_7^-	$\pi f_{7/2}\nu d_{5/2}$[a]	2760	2765	56.63
5_3^+	$\pi i_{13/2}\nu i_{11/2}$	2815	2780	53.16
			2807	
3_6^-	$\pi f_{7/2}\nu d_{5/2}$	2903	2850	23.54
			2883	
6_4^+	$\pi f_{7/2}\nu j_{15/2}$[a]	2978	2910	89.66
3_7^-	$\pi f_{7/2}\nu d_{5/2}$	2980	2962	43.32
			2979	
5_4^+	$\pi f_{7/2}\nu j_{15/2}$	2958	2996	52.01
			3023	
			3047	
			3097	
			3120	
6_7^-	$\pi h_{9/2}\nu d_{3/2}$	2873	3140	61.23
4_9^-	$\pi h_{9/2}\nu d_{3/2}$	3236	3182	72.33
5_9^-	$\pi f_{5/2}\nu g_{9/2}$	3169	3236	66.52
7_7^-	$\pi h_{9/2}\nu g_{7/2}$	3145	3244	93.58
3_9^-	$\pi h_{9/2}\nu d_{3/2}$	3193	3260	63.92
4_{10}^-	$\pi f_{5/2}\nu g_{9/2}$	3243	3319	60.27
4_{11}^-	$\pi f_{7/2}\nu s_{1/2}$	3395	3326	58.88
6_9^-	$\pi f_{5/2}\nu g_{9/2}$	3335	3394	62.96
3_{10}^-	$\pi f_{7/2}\nu s_{1/2}$	3408	3444	65.29
5_{11}^-	$\pi i_{13/2}\nu j_{15/2}$	3522	3530	74.47
4_5^+	$\pi i_{13/2}\nu d_{5/2}$	3648	3662	97.10
6_{11}^-	$\pi i_{13/2}\nu j_{15/2}$	3720	3692	88.50
4_{14}^-	$\pi f_{7/2}\nu g_{7/2}$	3933	3879	63.58
3_{14}^-	$\pi f_{7/2}\nu d_{3/2}$	3923	3900	82.77
5_{16}^-	$\pi f_{5/2}\nu i_{11/2}$	4286	4221	90.20

[a]This leading configuration differs from NNDC assignment. See text for details.

A. States below 2 MeV

In this energy range the agreement between experiment and theory is very good. Almost all states are reproduced by the calculations within a few keV, as shown in Table III. One should keep in mind, however, that this agreement arises from the fact that the two-body matrix elements of the interaction which was used were fitted to the energies of the states known in ^{210}Bi below 2 MeV. Many of the excitations, in spite of serving as an input to establish the shell-model interaction, had the spin-parity quantum numbers only tentatively assigned. In the present work, as discussed in Sec. II, by considering the observed decay paths and the results of the γ-ray angular correlations analysis we were able to make firm spin-parity assignments to most of the levels with uncertain quantum numbers: 563, 972, 993, 1209, 1248, 1524, 1777, and 1981 keV (see Table III).

In the 0- to 2-MeV energy range, two new excitations have been presently established, at 1527 and 1904 keV. Moreover, the presence of the state at 1197 keV was confirmed. It was previously located based on the observation of feeding primary γ ray [5]; however, its decay was not reported. The tentative values of spins (7^-, 3, and 1 or 2, respectively) could be assigned to them based on the observed decay pattern and the results of angular correlations. As it is not expected to see in this energy range states of any other nature than valence-particle excitations, we came to the following conclusions.

The state at 1197 keV may be connected to the theoretical 1^- at 1165-keV excitation, because the experimental 1165-keV level (reported in Ref. [5]) is not seen in our coincidence data.

The 1527-keV level may be connected to the theoretical state at 1383 keV with spin-parity 7^-, because the previously reported experimental partner is not present in our EXILL data, although for this spin range it should be observed.

Finally, concerning the 1904-keV level: We do not observe the 1897-keV state [3] assigned previously as 3^+, so we would rather connect our 1904-keV excitation to the 3^+ state predicted at 1898 keV.

In Table III, for each calculated state the leading configuration given by the shell model is shown. Although the model reproduces perfectly the experimental energies of the states below 2 MeV, as previously mentioned, in few cases (marked by the stars in Table III) the leading configuration is different from the one reported in National Nuclear Data Center (NNDC). This is not a surprise since configurations given by NNDC were proposed on the basis of different shell-model calculations in which original Kuo-Herling interactions were used. At the same time we are aware of the fact that experimental data on l transfer, from (d,p) and (α,d) measurements, exist for the 972- and 1248-keV levels. In the case of the 972-keV level, a tentative $l = 6$ is reported in NNDC, while our shell-model calculations suggest strong mixing of $l = 4$ and $l = 6$ configurations (with 43.85% and 36.68% admixture, respectively). On the contrary, in the case of the 1248-keV level the present shell-model calculations agree with the tentative $l = 4$ assignment from (d,p) data.

B. States above 2 MeV

The agreement between experiment and theory in the lower part of the scheme suggests that also at higher excitation energy the calculations should perform rather well.

The correspondence between experimental states and the results of calculations is shown in Fig. 9; it was established based on spin-parity assignments that were done or confirmed in the present work (for 15 levels) and identifications known from previous studies of ^{210}Bi. All of the states calculated in the energy region 1950-2845 keV, for spins 3–7, have their experimental counterparts. The average energy difference between computed and experimental values is 43 keV. This agreement provides additional confidence in the tentative spin-parity assignments. The energy-spin distribution of states populated in the decay following cold-neutron capture on ^{209}Bi, and having their calculated counterparts, is shown in Fig. 10. It is clearly seen that the decay favors excitations with spins $3\hbar$–$6\hbar$; this evidently results from the fact that the capture state can have spin-parity of 4^- or 5^-.

The detailed comparison between shell-model calculations and our experimental data allows to draw the following conclusions on the proton-neutron multiplets identification. All the members of the multiplet arising from the $\pi h_{9/2}\nu g_{9/2}$ configuration, i.e., 10 states with spins 0–9 and negative parity, were observed. Moving up with the excitation energy, the states involving the neutron promoted to the $i_{11/2}$ state or the proton to the $f_{7/2}$ orbital are present. Indeed, the multiplet $\pi h_{9/2}\nu i_{11/2}$ is represented by the 563-, 1175-, 1336-, 1390-, and 1981-keV states, while the configuration $\pi f_{7/2}\nu g_{9/2}$ is associated with the 916-, 972-, 1209-, 1248-, and 1464-keV levels. The members of the three multiplets mentioned above are of negative parity, but the higher-lying part of the ^{210}Bi level scheme includes also the positive-parity states, involving $\pi h_{9/2}\nu j_{15/2}$, $\pi i_{13/2}\nu g_{9/2}$, $\pi i_{13/2}\nu i_{11/2}$, $\pi i_{13/2}\nu s_{1/2}$, $\pi f_{7/2}\nu j_{15/2}$, and $\pi i_{13/2}\nu d_{5/2}$ configurations. Thus, the states identified in this work have configurations which arise from neutron and proton promotions to almost all orbitals available above the ^{208}Pb core, allowed by the Kuo-Herling model space.

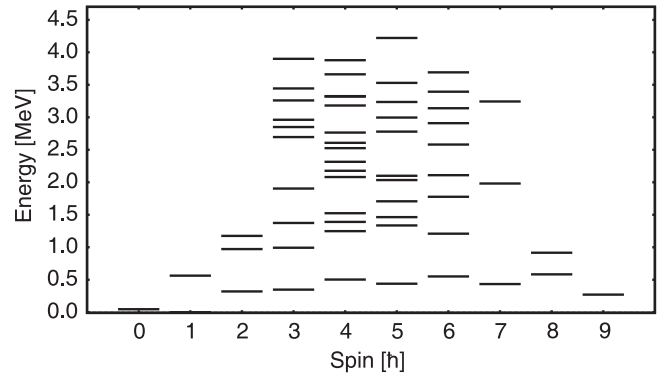

FIG. 10. The energy-spin distribution of states observed in the decay following cold-neutron capture on ^{209}Bi and having their calculated counterparts.

As can be seen in Fig. 9, some of the levels which have been located in ^{210}Bi above 2 MeV do not have their theoretical counterparts; they are marked with a star. These are the previously known excitation at 2007 keV and newly found states at 2147, 2556, 2726, 2730, 2807, 2883, 2979, 3023, 3047, 3097, and 3120 keV. The 12 experimental levels in the energy range of 2.0–3.1 MeV cannot have theoretical partners within this model space, because all calculated states within this energy range were already assigned to other excitations. As excitations to orbitals outside this model space require much higher energies, it is clear that these nonassigned states must be of other-than-shell-model origin. Therefore, it is most natural to consider these states as arising from the couplings of one-proton one-neutron excitations to the octupole vibration of the ^{208}Pb core at 2615 keV. Indeed, within a weak-coupling approach one may expect several states arising from the coupling of the 3^- phonon to the lowest excitations in ^{210}Bi, i.e., $1^-, 0^-, 9^-, 2^-$, and 3^-. This coupling would give a number of positive-parity states characterized by spin values between 2 and 12 and located around 2.6 MeV, although splitting of the order of hundreds of keV or more can be expected [22–26]. The 12 unassigned states, mentioned above, could be of this origin. To confirm this hypothesis, lifetime measurements would be needed.

IV. CONCLUSIONS

A study of low-spin states in ^{210}Bi populated in a cold-neutron capture reaction was performed with unprecedented sensitivity by employing the coincidence technique and the EXILL HPGe array [9]. As the result, the decay scheme was established for a total number of 70 states, of which 33 are new. For a large number of levels, spins and parities were assigned with the help of γ-ray angular correlations. To a few

excitations, known from previous works in the lower part of the scheme, new quantum numbers assignments have been proposed. The shell-model calculations which involve only the valence proton and neutron excitations and use the Kuo-Herling interactions have been performed. It has been found that the observed states arise from the promotion of a proton and neutron to almost all the orbitals which are available in the model space used, i.e., above the ^{208}Pb core.

All of the states calculated in the energy region 0–1950 keV, for the spin range 0–8, and 1950-2845 keV, for spins 3–7, have their experimental counterparts. However, not all observed excitations in these energy and spin regions have a corresponding calculated level. Indeed, around the energy of 2.6 MeV and spins $2\hbar$–$8\hbar$, one may expect presence of states which arise from couplings of the ground state or of the lowest excited states of ^{210}Bi to the 3^- octupole vibration in ^{208}Pb, at 2615 keV. The states located at 2007, 2147, 2556, 2726, 2730, 2807, 2883, 2979, 3023, 3047, 3097, and 3120 keV, which do not have a calculated partner, very likely are these particle-phonon excitations. Such excitations may serve as a testing ground for new models which aim at describing particle-phonon couplings on microscopic basis [27].

Within the presented work, we have also performed an analysis aimed at establishing the spin-parity quantum numbers of the neutron capture state at 4605 keV in ^{210}Bi. The decay pattern and the results of angular correlations analysis obtained for the strong γ rays deexciting the capture state clearly indicate that it consists of at least two states with J^π values of 4^- and 5^-.

The present work demonstrates that a study of γ decay from a neutron capture state performed with an efficient Compton-suppressed germanium array makes it possible, for certain nuclei, to make complete spectroscopy of a wide energy and spin range. This very extensive structural data can then be used for detailed tests of models which aim at providing a complete description of the excited states up to a few MeV. Additionally, it can serve as an input for further improvements of shell-model effective interactions in the vicinity of ^{208}Pb, which would allow to extend our understanding of nuclear structure towards heavier nuclei in the northeast quadrant.

ACKNOWLEDGMENTS

The authors thank the technical services of the ILL, LPSC, and GANIL for supporting the EXILL campaign. The EXOGAM Collaboration and the INFN Legnaro are acknowledged for the loan of Ge detectors. This work is supported by the Polish National Science Centre under Contracts No. DEC-2011/01/N/ST2/04612, No. 2014/14/M/ST2/00738, and No. 2013/08/M/ST2/00257.

[1] J. R. Erskine, W. W. Buechner, and H. A. Enge, Phys. Rev. **128**, 720 (1962).
[2] C. V. K. Baba, T. Faestermann, D. B. Fossan, and D. Proetel, Phys. Rev. Lett. **29**, 496 (1972).
[3] http://www.nndc.bnl.gov/nudat2/; http://www.nndc.bnl.gov/ensdf/ensdf/ensdf.jsp
[4] N. Cieplicka *et al.*, Acta Phys. Pol. B **45**, 205 (2014).
[5] R. K. Sheline, R. L. Ponting, A. K. Jain, J. Kvasil, B. bu Nianga, L. Nkwambiaya, Czech. J. Phys. B **39**, 22 (1989).
[6] J. S. Tsai, T. J. Kennett, and W. V. Prestwich, Phys. Rev. C **27**, 2397 (1983).
[7] A. Borella, T. Belgya, S. Kopecky, F. Gunsing, M. Moxon, M. Rejmund, P. Schillebeeckx, and L. Szentmiklési, Nucl. Phys. A **850**, 1 (2011).
[8] G. Audi, A. H. Wapstra, and C. Thibault, Nucl. Phys. A **729**, 337 (2003).
[9] M. Jentschel *et al.* (unpublished).
[10] H. Abele *et al.*, Nucl. Instrum. Methods A **562**, 407 (2006).
[11] J. Simpson, F. Azaiez, G. de France, J. Fouan, J. Gerl, R. Julin, W. Korten, P. J. Nolan, B. M. Nyako, G. Sletten, P. M. Walker, and the EXOGAM Collaboration, Acta Phys. Hung. N.S., Heavy Ion Phys. **11**, 159 (2000).
[12] http://gasp.lnl.infn.it/
[13] P. Mutti, A. Blanc, G. de France, M. Jentschel, U. Köster, E. Ruiz Martinez, G Simpson, T. Soldner, C. A. Ur, and W. Urban, in *Advancements in Nuclear Instrumentation Measurement Methods and their Applications (ANIMMA), 2013 3rd International Conference on, Marseille, 2013* (IEEE, Marseille, 2013), p. 1.
[14] P. Merlotti, Study of the ^{209}Bi$(n,\gamma)^{210}$Bi Reaction with Spectroscopy Techniques at High Energy Resolution, Master's thesis, University of Milan, 2013.
[15] H. Morinaga and T. Yamazaki, *In-beam Gamma-ray Spectroscopy* (North-Holland, Amsterdam, 1976).
[16] A. J. Ferguson, *Angular Correlation Methods in Gamma-ray Spectroscopy* (North-Holland, Amsterdam, 1965).
[17] N. Cieplicka-Oryńczak (unpublished).
[18] J. J. Bosman and H. Postma, Nucl. Instrum. Methods **148**, 331 (1978).
[19] B. A. Brown, A. Etchegoyen, N. S. Godwin, W. D. M. Rae, W. A. Richter, W. E. Ormand, E. K. Warburton, J. S. Winfield, L. Zhao, and C. H. Zimmerman, MSU-NSCL Report No. 1289, 2004.
[20] T. T. S. Kuo and G. Herling, U. S. Naval Research Laboratory Report No. 2258, 1971; G. Herling and T. T. S. Kuo, Nucl. Phys. A **181**, 113 (1972).
[21] E. K. Warburton and B. A. Brown, Phys. Rev. C **43**, 602 (1991).
[22] A. Bohr and B. R. Mottelson, *Nuclear Structure* (World Scientific, Singapore, 1998).
[23] D. Montanari *et al.*, Phys. Lett. B **697**, 288 (2011).
[24] D. Montanari, S. Leoni, D. Mengoni, J. J. Valiente-Dobon, G. Benzoni, N. Blasi, G. Bocchi, P. F. Bortignon, S. Bottoni, A. Bracco, F. Camera, P. Casati, G. Colo, A. Corsi, F. C. L. Crespi, B. Million, R. Nicolini, O. Wieland, D. Bazzacco, E. Farnea, G. Germogli, A. Gottardo, S. M. Lenzi, S. Lunardi, R. Menegazzo, G. Montagnoli, F. Recchia, F. Scarlassara, C. Ur, L. Corradi, G. de Angelis, E. Fioretto, D. R. Napoli, R. Orlandi, E. Sahin, A. M. Stefanini, R. P. Singh, A. Gadea, S. Szilner, M. Kmiecik, A. Maj,

W. Meczynski, A. Dewald, T. Pissulla, and G. Pollarolo, Phys. Rev. C **85**, 044301 (2012).

[25] G. Bocchi, S. Leoni, S. Bottoni, G. Benzoni, A. Bracco, P. F. Bortignon, G. Colo, B. Belvito, C. R. Nita, N. Marginean, D. Filipescu, D. Ghita, T. Glodariu, R. Lica, R. Marginean, C. Mihai, A. Negret, T. Sava, L. Stroe, S. Toma, D. Bucurescu, I. Georghe, R. Suvaila, D. Deleanu, C. A. Ur, and S. Aydin, Phys. Rev. C **89**, 054302 (2014).

[26] C. R. Nita, D. Bucurescu, N. Marginean, M. Avrigeanu, G. Bocchi, S. Bottoni, A. Bracco, A. M. Bruce, G. Cata-Danil, G. Colo, D. Deleanu, D. Filipescu, D. G. Ghita, T. Glodariu, S. Leoni, C. Mihai, P. J. R. Mason, R. Marginean, A. Negret, D. Pantelica, Z. Podolyak, P. H. Regan, T. Sava, L. Stroe, S. Toma, C. A. Ur, and E. Wilson, Phys. Rev. C **89**, 064314 (2014).

[27] G. Colò, H. Sagawa, and P. F. Bortignon, Phys. Rev. C **82**, 064307 (2010); G. Colò (private communication).